# CONTENTS

# CHAPTER 2

# PHOTOPOLYMERISATION OF $C_{60}$ PROBED BY SECOND HARMONIC GENERATION

## 2.1 Introduction

Polymerisation can be induced in solid $C_{60}$ by photoirradiation, electron or ion impact, by high pressure and temperature, by doping with alkali metals or by mechanochemical reactions [EkR00]. Photopolymerisation occurs whenever the material is irradiated with ultraviolet or visible light and it renders the $C_{60}$ films insoluble in toluene, a property that suggests lithographic applications, since the unexposed regions of the films remain soluble in toluene. The process is reversible upon prolonged heating of the films above 100 °C [EkR00]. $C_{60}$ photopolymerisation was first described by Rao et al. [RZW93] as a 2+2 cycloaddition process, leading to covalent cross-linking bonds. Mechanical [TSK97, TKS98], optical [RZW93, MOY97] and other properties of the polymeric phase of $C_{60}$ were investigated by different groups. The polymeric phase is harder than the pristine phase, as shown by the indentation of a diamond pyramidal tip into the film [TSK97, TKS98]. The maximum number of 2+2 intermolecular bonds that one molecule can form was found by X-ray photoelectron spectroscopy to be six [OnT97]. Raman spectroscopy was by far the most intensely used method for the characterisation of the phototransformation process [ZRW92, RZW93, WHD93, ZDR93, WHB94, ERZ95, BWK96, MOY97, PHK98, SIN01]. For $C_{60}$, a molecule with $I_h$ symmetry, only 14 vibrational modes are optically active. Essentially all vibrational modes of the $(C_{60})_N$ oligomers become either Raman- or IR-active, because of the symmetry lowering of the phototransformed fullerene phases through the intermolecular covalent bonding. Due to its very high sensitivity to photopolymerisation, the most intensively studied vibration is the $A_g(2)$ pinch mode observed at 1469 $cm^{-1}$ for pristine $C_{60}$. Although the 2+2 covalent bonding between the fullerene cages has been calculated to be the most stable configuration of the $C_{60}$-$C_{60}$ dimers

[SMX93, MSS94], the detailed mechanisms of the photoinduced formation of intermolecular covalent bonds is still under debate.

The $C_{60}$ photopolymerisation process is studied here by Second Harmonic Generation, a method which is very sensitive to structural and chemical modifications in the films. An outline of the different mechanisms proposed for the photopolymerisation, and of the reported studies on the reaction kinetics, is given in Section 2.2 of this chapter. The theory of Second Harmonic Generation from thin films is discussed in Section 2.3. The experimental setup used for the present measurements is shown in Section 2.4. Results of the photopolymerisation kinetics of crystalline $C_{60}$ films, combined with infrared spectroscopic studies of the phototransformed phase, are discussed in the following section. The effect of the photoirradiation on $C_{60}$ films with a high content of oxygen impurity is presented in Section 2.6, and the conclusions are given in Section 2.7.

## 2.2 The $C_{60}$ photopolymerisation process

### 2.2.1 The 2+2 cycloaddition

The 2 + 2 cycloaddition is a known photochemical mechanism leading to the covalent attachment of adjacent, typically organic molecules [VeR91]. The reaction involves the reconfiguration of double bonds (C = C), one on each molecule, which are oriented parallel to each other and separated by less than ~ 4.2 Å. From symmetry considerations, expressed by the Woodward-Hoffman rules, such reaction is possible only with photochemical assistance. Both double bonds are broken and reform as a four-sided ring (Fig.2.1) [VeR91]. This mechanism is particularly active in the solid state, where the molecules are confined in close proximity.

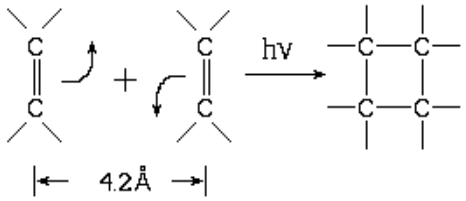


*Fig.2.1. Schematics of the 2 + 2 cycloaddition reaction between parallel carbon double bonds on adjacent molecules [VeR91]*

Two $C_{60}$ molecules can dimerise by this 2 + 2 cycloaddition mechanism, as shown in Fig.2.2. In solid $C_{60}$, which crystallises in an fcc lattice, adjacent molecules are separated by as little as 3.5 Å [DDE96].

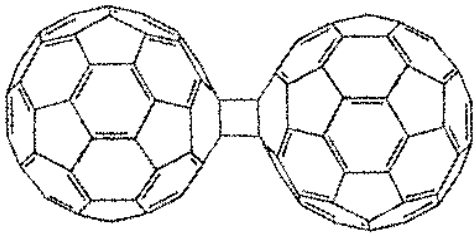

*Fig.2.2. $C_{60}$ dimer produced by the photochemical 2 + 2 cycloaddition reaction*

The molecules, each containing 30 double bonds, are freely spinning about their lattice positions at temperatures higher than the orientational ordering temperature (260 K). They can adopt 900 favourable orientations, which could promote the 2 + 2 cycloaddition reaction. Temperature dependent studies of the photopolymerisation have shown that the process takes place mainly between 260 K [ZDR93, BWK96] and 400 K [BWK96]. Below 260 K the molecules lose two of their three degrees of rotational freedom and therefore the double bonds on adjacent $C_{60}$ are less likely to be parallel. At 90 K the rotation of the molecules is completely frozen. In this low-temperature phase electron-rich double bonds on one $C_{60}$ molecule are centred opposite electron-deficient rings on the adjacent molecules (83% will oppose a pentagon and 17% a hexagon). The low temperature limit for the photopolymerisation is thus imposed by simple geometrical reasons. At temperatures higher than ~ 375 K the transformation process is slowed down, possibly due to the larger lattice constant. In addition, the polymerisation is thermally reversible. An activation energy of 1.25 eV, interpreted as the thermal barrier for the dissociation of a monomer from a dimer or higher oligomer, was obtained by studying the evolution of the $A_g(2)$ Raman mode with the heating temperature of initially photopolymerised films [WHB94].

## 2.2.2 The triplet state and the reaction path

The first reaction scheme proposed for $C_{60}$ photopolymerisation by Wang et al [WHD93] is depicted in Fig.2.3. The incident photons are preparing molecules in the lowest excited triplet state ($T_1$) via singlet state absorption ($S_0 \rightarrow S_n$) followed by internal conversion and intersystem crossing. The excited molecule reacts with an adjacent molecule that remains in the singlet ground state ($S_0$). Three photophysical properties of $C_{60}$ are required to achieve a significant population of the $T_1$ state by optical pumping: (1) dipole-allowed transitions from the ground state to excited singlet states (observed above ~ 1.7 eV in the case of solid $C_{60}$ [DDE96]); (2) a

nearly 100% efficient intersystem crossing [ERZ95] and (3) a sufficiently long $T_1$ lifetime (tens of milliseconds [DDE96]).

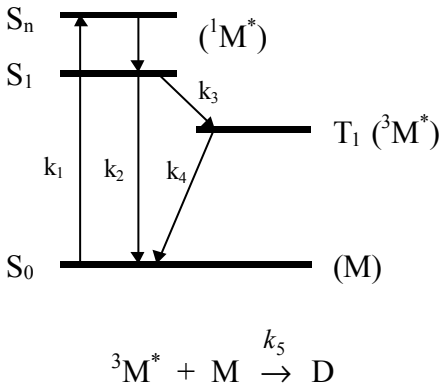


*Fig.2.3. Schematic energy level diagram for the $C_{60}$ monomer, illustrating the path that is leading to the bimolecular photochemical reaction of a $C_{60}$ monomer in the excited triplet state ($^3M^*$) with a monomer in the ground state (M) to form a dimer (D) [WHD93]*

The rate k dominating the phototransformation is directly related to the one describing the optical pumping, under the following assumptions: (1) the internal conversion rate constants for $S_n \rightarrow S_1$ are ignored (since the process is very fast), (2) a low quantum yield for singlet exciton recombination (~ 0.07%, as reported in ref. [LSN92]) and a nearly 100% efficient intersystem crossing ($k_2 << k_3$), (3) since the triplet state has a long lifetime, $k_4 << k_5 M(t)$. Finally, the density of monomers decreases as $M(t) \sim M_0 \cdot \exp(-2k_1 t)$ and one photon absorbed with a rate $k_1$ causes the loss of two monomers, with a rate constant $k = 2k_1$ for the loss of monomers, producing one dimer.

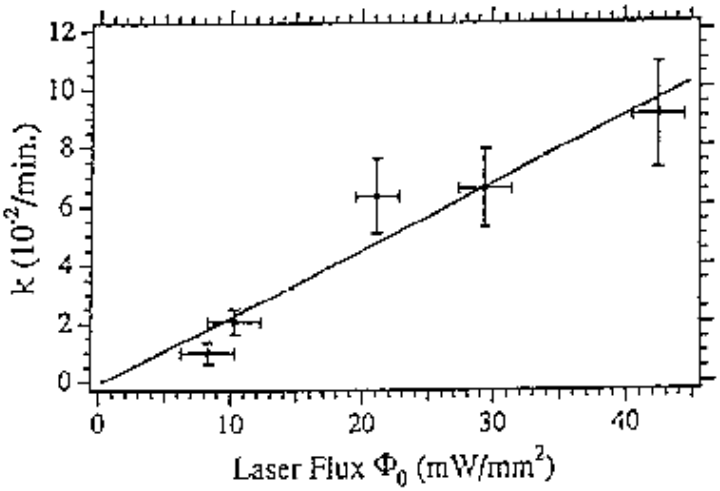


*Fig.2.4. Rate constant ($k = 2k_1$) for the photodimerisation of $C_{60}$ as a function of the flux density of 488 nm laser irradiation. The straight line is a result of a least-squares fit to the data [WHD93]*

The light intensity dependence of the photopolymerisation rate constant k reported in [WHD93] (shown in Fig.2.4) remains, at least to our knowledge, the only one of its kind published so far in the literature and the given interpretation has been generally accepted in most further studies.

Oxygen intercalation in the $C_{60}$ lattice was found to harden the material against photopolymerisation [ZRW92]. This observation was interpreted as evidence that the $T_1$ state is involved in the photoreaction of $C_{60}$, since the interaction with the $O_2$ $^3S$ state is known to efficiently quench the $T_1$ state.

Photoinduced absorption measured from $C_{60}$ films, however, showed no absorption band due to the triplet state of the molecule, in contrast to the observation for $C_{60}$ solutions. This is an indication that the relaxation of the excitations in the molecular solid follows a different path than the intersystem crossing, to be discussed next.

### 2.2.3 The charge transfer exciton reaction scheme

Contraction of the intermolecular separation in the $C_{60}$ solid was proposed to be the trigger mechanism initiating the polymerisation. The polymerisation of $C_{60}$ can be achieved by high pressure (which intrinsically contracts the intermolecular distance) and by alkali metal doping, where the Coulomb interaction between the metal ions and the $C_{60}$ anions has been proposed to drive a lattice distortion leading to chain polymerisation. For the photopolymerisation, this brings the charge transfer (CT) excitons into discussion, due to their strong interaction with the lattice phonons.

In a molecular crystal such as $C_{60}$, the photoexcitation creates an electron and a hole bound to each other by the Coulomb interaction, thus creating an exciton. Two types of excitons can be distinguished: the Frenkel excitons, where the electron-hole pair is localised on one molecule creating an intramolecular excited state, and the CT excitons, where the electron and the hole are split on two adjacent molecules, and they interact through the Coulomb force to form the intermolecular excitonic state. The interaction between the CT exciton and the lattice phonons is strong compared with the case of Frenkel excitons. Calculations have shown that near the absorption edge (~1.7 eV) the excitations are rather localised on a single molecule (Frenkel excitons), while at energies 2.33 eV and above, the excitons begin to take on charge transfer character [TsN94]. By comparing the absorption spectrum of the ideal $C_{60}$ molecular solid - based on the molecular polarizability of $C_{60}$ - and the absorption of the real solid, Holden and Ecklund (Chapt.4.4.4. in ref.[EkR00]) found a new broad resonance between 2.5 and 3.1 eV, which they assigned to the CT excitons. Using electroabsorption, luminescence and its

modulation by an external electric field, Kazaoui et al. [KMT98] have assigned the most significant CT states at 2.43 and 3.5 eV.

The relaxation of these excitons can follow different paths: intramolecular relaxation, exciton-exciton annihilation, free carrier generation, radiative recombination, self-trapping etc. The self-trapping of the charge transfer excitons is of particular interest for our discussion. Due to the strong interaction with phonons, the exciton becomes localised and can be self-trapped in the potential well associated with the local lattice distortion that is induced by the exciton itself. Nakamura et al. [ISY96, NIY96, INS98] have studied the relaxation dynamics of the 3 eV photoexcitation in $C_{60}$ thin films of 150 monolayers (ML) by transient absorption in the region 2.3-2.8 eV (associated with the CT states). A fast relaxation within 1 ps was observed and interpreted as self-trapping of the CT excitons. An inter-molecular type of triplet state was associated with this self-trapped CT state, with a lifetime of almost 50 ms.

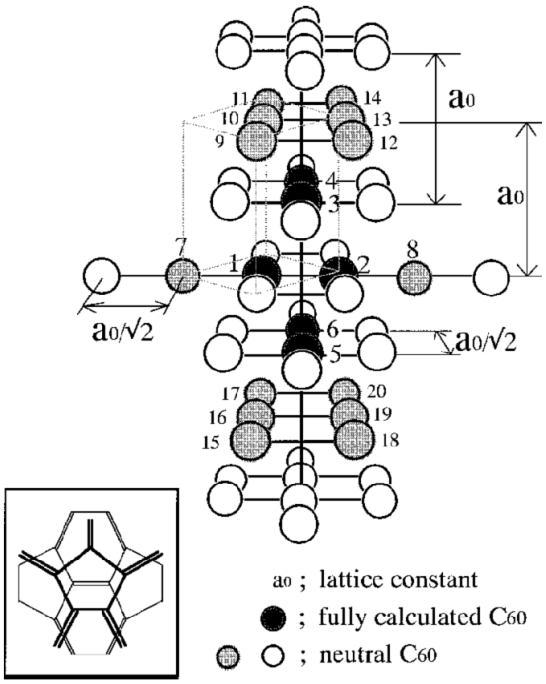


*Fig.2.5. Schematics of the 54 $C_{60}$ molecules considered in the calculation, arranged on the fcc lattice points. Black circles: molecules assumed to have excited states of $\pi$ electrons. The molecules labelled 1 and 2 are assumed to dimerise. Grey circles: molecules in ground state, displaced during the dimerisation. Open circles: ground state molecules keeping their fcc lattice points. Inset: the relative orientation of the molecules at the beginning of the reaction [SIN00].*

Suzuki et al. [SIN00] investigated in a theoretical study the lattice relaxation of photogenerated excitons in crystalline $C_{60}$. By analysing the adiabatic potential energy surfaces of the Frenkel and CT excitons, they show that the CT exciton relaxes down to a self-trapped state, causing a local distortion of the lattice. From the 54 $C_{60}$ molecules considered in the

model, 20 molecules (including the two involved in the CT exciton) will suffer a displacement, conventionally considered towards the centre of the cluster (Fig.2.5): $\Delta R_{1,2}$ = 0.65 Å, $\Delta R_{7,8}$ = 0.47 Å, $\Delta R'_{3\text{-}6}$ = -0.20 Å and $\Delta R_{9\text{-}20}$ = -0.14 Å. The two central molecules will rotate (when the temperature is higher that $T_c$ = 260 K) to the orientation with the double bonds parallel to each other during the approach by $\Delta R$ = 0.8 Å ($\Delta R'$ = 0.20 Å), the distance regarded as the "reaction point".

Once the double bonds are broken to form the 2+2 intermolecular bonds, the molecules will relax to $\Delta R$ = 0.65 Å, with a deformation of the two fullerene cages forming the dimer. An energy barrier of 2.5 eV between the fcc crystal and the dimer was computed. Since this energy is generally higher than the energy of the relaxed excitons, they consider that multiphotons are needed to achieve dimerisation. While this result determined theoretical studies with rather spectacular results, like the need of $10^5$ photons to create one single bond [Mak01], so far it has not been confirmed experimentally.

### 2.2.4 Kinetics of phototransformation

The kinetics of the photopolymerisation was studied mainly by Raman spectroscopy [ZRW92, WHD93, ZDR93, WHB94, ERZ95, BWK96, MOY97, PHK98, SIN01], but also by optical absorption [MOY97], photoelectron spectroscopy [OnT97] or mechanical indentation [TSK97, TKS98]. Despite the large number of studies dedicated to the phototransformation kinetics, little is known about the kinetics in the initial phase of irradiation. The preparation conditions for the $C_{60}$ films or crystals varied largely in these different experiments and the film quality may have an influence on the reaction kinetics [WHB94]. The photoelectron spectroscopy study was mainly concerned with the number of 2+2 cross-links between adjacent $C_{60}$ molecules formed in saturation. The maximum number of intermolecular bonds was found to be 6, and the saturation was reached after ~350 hours of irradiation with a mercury lamp, with an average power of 0.15-0.20 W/cm$^2$ [OnT97]. It is important to note that the films in this study from Onoe and Takeuchi were exposed to air.

In Raman studies, the reaction is induced by the relatively intense Raman laser itself. The early stages of the transformation in oxygen-free samples at room temperature are thus difficult to observe. A first kinetics study was presented by Wang et al. [WHD93] on films of $C_{60}$ irradiated under He atmosphere with an $Ar^+$ laser at 488 nm, with an intensity of 0.83 W/cm$^2$. The phototransformation was monitored by the shift of the $A_g(2)$ pentagonal pinching mode from 1469 cm$^{-1}$, corresponding to the pristine $C_{60}$, to 1459 cm$^{-1}$ - assigned here to a general

polymeric phase. The transformation showed an exponential behaviour, with a time constant of about 150 minutes, equivalent to about $10^{22}$ photons/cm$^2$. The polymeric peak appears only after 20 minutes of irradiation (~$10^{21}$ photons/cm$^2$), while the transformation is completed (by the total suppression of the monomeric peak) after 600 minutes of irradiation. Burger et al. [BWK96] compared the Raman spectra of single crystals (transported through air) irradiated at different temperatures, between 27 and 180 °C to obtain spectroscopic information on the initial products of the phototransformation. The transformation was considerably retarded for elevated temperatures so that the early stages could be observed. The calculations from Porezag et al. [PPF95, PJF97] were used to identify the structures formed at higher temperatures as dimers. These calculations are clarifying the position of the $A_g(2)$ mode for the monomers (1469 cm$^{-1}$), dimers (1459-1462 cm$^{-1}$) and higher oligomers (1450-1459 cm$^{-1}$) (see Fig.2.6).

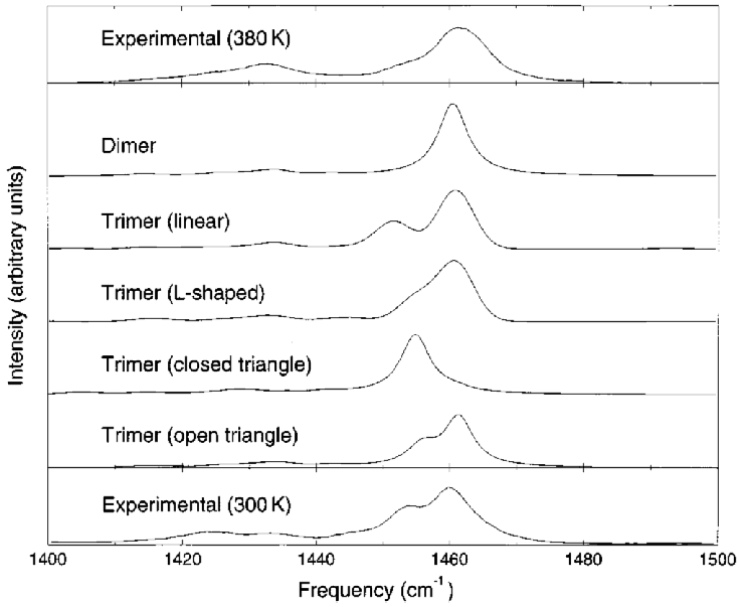


*Fig.2.6. Experimental Raman spectra in the pentagonal pinch mode region [BWK96] in comparison with the calculations of Porezag et al. [PJF97].*

Park et al [PHK98] studied in situ under ultra high vacuum (UHV) conditions the transformation kinetics of the dimers into higher oligomers, on films of different thickness, under irradiation with an $Ar^+$ laser at 514.5 nm, with 1200 W/cm$^2$. The peak corresponding to the $C_{60}$ monomer disappeared "instantaneously" when irradiating the films at room temperature, so that only the evolution of the dimers into higher oligomers was followed. When the samples were heated at 150 °C during the phototransformation, the evolution of this monomeric peak could be studied together with the dimeric and higher polymeric phases.

The irradiation conditions varied largely in the different studies presented in the literature. While for irradiation with mercury or xenon lamps the average power on the sample was usually

low (0.02-0.20 W/cm$^2$ [TSK97, TKS98, OnT97]), the intensities used from $Ar^+$ lasers were in general considerably higher: 2000 W/cm$^2$ in ref.[MOY97], 4 W/cm$^2$ in [ZDR93], 60 W/cm$^2$ in [BWK96], 75 W/cm$^2$ in [ZRW92] and so on. Quite recently, Sakai et al. [SIN01] showed that the laser used for irradiation also heats the film so to cause the thermal destruction of the photogenerated polymers, when using power densities of 7 W/cm$^2$ and higher.

It is important to note that no experiment involving Raman spectroscopy was reported on the transformation of oxygen-free crystalline films at room temperature, for irradiation doses lower than $10^{21}$ photons/cm$^2$. An interesting study of the microhardness of the films measured as a function of the irradiation time was reported by Tachibana et al. [TSK97, TKS98]. The hardness of the films increased with the irradiation time and reached saturation after only 6 x $10^{20}$ photons/cm$^2$. The experiments were performed in air. Although the increase in the hardness was attributed to the polymerisation of the films, the influence of the oxygen present in the films and possible oxidation reactions were not considered. The diffusion of the oxygen into the films under irradiation with light and eventually the oxidation of the molecules were confirmed by Raman spectroscopy and Rutherford backscattering analyses [WHB94, ERZ95].

In the present study, we chose the second harmonic generation (SHG) at 1064 nm as a probe for the photopolymerisation kinetics. The 1064 nm wavelength is far from the absorption edge of $C_{60}$, so that the probe does not interfere with the photoreaction.

## 2.3 Second Harmonic Generation in $C_{60}$ films

The $C_{60}$ is a centrosymmetric molecule crystallising in an fcc lattice that also has inversion symmetry. Both macroscopic and microscopic electric dipole contributions from the bulk of the $C_{60}$ film to second harmonic generation are therefore forbidden. The weak signals that can be generated by such films should be attributed to the interfaces with the substrate and the vacuum, where the symmetry is broken by the local environment. However, even in centrosymmetric media, nonlocal electric-quadrupole and magnetic-dipole contributions can arise from the bulk of the films giving surprisingly high SH signals. While Hoshi et al [HNM91] were the first ones to report SHG from $C_{60}$, Wang et al [WZL92] made the first attempt to assign the origin of the SH signal from $C_{60}$ films in air, at 1064 nm fundamental wavelength. Following a similar analysis as the one first reported by Koopmans et al [KJJ93, Koo93] for the SH generated from $C_{60}$ films at 688 nm, Wilk et al. [WJS95] have shown that there is a strong bulk contribution to the SH generated by a YAG laser at 1064 nm, of electric quadrupole nature. Theoretical

calculations [QYS93, MSB98] also confirmed these experimental results. Some aspects of the theory for the second harmonic generated from a thin film of $C_{60}$ at 1064 nm are summarised in the following chapter.

### 2.3.1 SHG from an isotropic film

The optical response of a medium is described by the induced polarisation density ***P***. Within the electric dipole approximation, the polarisation can be written as an expansion of the electric field*:

$$\boldsymbol{P} = \vec{\chi}^{(1)} \cdot \boldsymbol{E} + \vec{\chi}^{(2)} : \boldsymbol{EE} + \vec{\chi}^{(3)} : \boldsymbol{EEE} + \ldots , \qquad (2.1)$$

where $\vec{\chi}^{(n)}$ is the n-th order susceptibility tensor of rank n+1. The number of independent and nonzero components of these tensors is restricted by the symmetry of the material under consideration. For materials with a centre of inversion, $\vec{\chi}^{(n)}$ is invariant under the transformation $\boldsymbol{r} \rightarrow \boldsymbol{-r}$; this gives $\vec{\chi}^{(n)} = (-1)^{n+1}\vec{\chi}^{(n)}$. Any even-order response is thus forbidden within the electric dipole (ED) approximation for a centrosymmetric material.

The rapid variation of the pump electric field at the interface between two centrosymmetric media will give rise to a second harmonic signal coming from the leading-order magnetic-dipole and electric-quadrupole terms. This nonlinearity was first treated as a sheet of generalised nonlinear source polarisation at the interface by Bloembergen and Pershan in 1962 [BlP62]. with the polarisation of this sheet determined only by nonlocal terms, based on bulk properties. Later on, it was recognised that the implicit broken symmetry of the surface should give rise to an ED-allowed surface SHG. The phenomenological description of SHG from centrosymmetric media was further improved by including the surface E1 susceptibility terms as sources for the polarisation sheet [SiS82, G-SC86, Hei91]. The radiation at the second harmonic frequency both in reflection and in transmission is obtained by solving Maxwell's equations with a nonlinear source polarisation $\boldsymbol{P}\ (x,y)\delta(z)$ in order to get the boundary conditions for the electric and magnetic fields on either side of this polarised sheet.

The invariance of the $\vec{\chi}_d^{(2)}$ under the symmetry operations of the $C_{\infty v}$ group to which an isotropic interface belongs leaves only three independent nonzero tensor elements (within the coordinates system from Fig.2.7): $\chi_{s,zzz}^{(2)}, \chi_{s,zxx}^{(2)} = \chi_{s,zyy}^{(2)}, \chi_{s,xzx}^{(2)} = \chi_{s,xxz}^{(2)} = \chi_{s,yzy}^{(2)} = \chi_{s,yyz}^{(2)}$.

* hereafter, the vectors will be denoted with bold characters "***A***", higher order tensors with "$\vec{\vec{B}}$" and the tensorial product with ":"

The nonlinear source polarisation in the bulk of a material, as a multipole expression in successive degrees of nonlocality, is:

$$\begin{aligned} \boldsymbol{P}^{nls}(\Omega) = \vec{\vec{\chi}}_d^{(2)}(\Omega=\omega_1+\omega_2):\boldsymbol{E}(\omega_1)\boldsymbol{E}(\omega_2) \; + \\ \frac{1}{2}\vec{\vec{\chi}}_q^{(2)}(\Omega=\omega_1+\omega_2):\boldsymbol{E}(\omega_1)\nabla\boldsymbol{E}(\omega_2) \; + \\ \frac{1}{2}\vec{\vec{\chi}}_q^{(2)}(\Omega=\omega_1+\omega_2):\boldsymbol{E}(\omega_2)\nabla\boldsymbol{E}(\omega_1) \; + \ldots . \end{aligned} \tag{2.2}$$

The relative contributions of the successive terms vary like ($ka$), with $a$ the typical atomic dimension. For centrosymmetric media, the leading-order response consists of the electric-quadrupole and magnetic-dipole terms comprised of products of $\boldsymbol{E}$ and the spatial derivatives of $\boldsymbol{E}$. The generalised polarisation can be expressed up to the first order spatial derivatives of the electric field like:

$$P^{(2)}(\Omega) = P_d^{(2)}(\Omega) - \nabla\cdot\vec{\vec{Q}}^{(2)}(\Omega) + \nabla\times M^{(2)}(\Omega) \; . \tag{2.3}$$

In the case of SHG, we can write:

$$\begin{aligned} \boldsymbol{P}_d^{(2)} &= \vec{\vec{\chi}}^{D}:\boldsymbol{E}(\omega)\boldsymbol{E}(\omega) + \vec{\vec{\chi}}^{P}:\boldsymbol{E}(\omega)\nabla\boldsymbol{E}(\omega) \\ \vec{\vec{Q}}^{(2)} &= \vec{\vec{\chi}}^{Q}:\boldsymbol{E}(\omega)\boldsymbol{E}(\omega) \\ \boldsymbol{M}^{(2)} &= \vec{\vec{\chi}}^{M}:\boldsymbol{E}(\omega)\boldsymbol{E}(\omega) \; , \end{aligned} \tag{2.4}$$

with $\vec{\vec{\chi}}^{D}$ describing a local response, while $\vec{\vec{\chi}}^{P}$, $\vec{\vec{\chi}}^{Q}$ and $\vec{\vec{\chi}}^{M}$ are nonlocal. For nonmagnetic materials (inversion symmetry in both space and time), $\boldsymbol{M}^{(2)}(\Omega) = 0$. The effective SH polarisation can be written as [G-SS88]:

$$P_i(\Omega) = \gamma\nabla_i(\boldsymbol{E}\cdot\boldsymbol{E}) + (\delta-\beta-2\gamma)(\boldsymbol{E}\cdot\nabla)E_i + \beta(\nabla\cdot\boldsymbol{E})E_i + \zeta E_i\nabla_i E_i \; . \tag{2.5}$$

For a homogeneous medium, $\nabla\cdot\boldsymbol{E} = 0$. The coefficients $\beta$, $\gamma$ and $\delta$ describe the isotropic response of the medium. These coefficients correspond to the non-vanishing tensor components of the susceptibility tensors (for an isotropic bulk) as follows: $\beta = 2(\chi^{P}_{iijj} - \chi^{Q}_{ijij}))$; $\gamma = \chi^{P}_{ijij} - \chi^{Q}_{iijj}$ ; $\delta = 2(\chi^{P}_{iiii} - \chi^{Q}_{iiii})$ and $\delta - \beta - 2\gamma = 2(\chi^{P}_{ijji} - \chi^{Q}_{ijij})$ . $\zeta E_i\nabla_i E_i$ is the only anisotropic term in this expression; for an isotropic material, $\zeta = 0$. When only a single plane wave is present in the medium (reflections from deeper lying interfaces are ignored) the term $(\delta-\beta-2\gamma)(\boldsymbol{E}\cdot\nabla)E_i$ vanishes. For a simple measurement of an isotropic medium (i.e. having only one interface between two centrosymmetric media), the only bulk term contributing to the signal remains $\gamma\nabla_i(\boldsymbol{E}\cdot\boldsymbol{E})$ which is a longitudinal field for any pump field $\boldsymbol{E}$, giving rise to radiation

fields indistinguishable from those of an equivalent surface nonlinear response [SMS87, G-SS88]. Therefore, SHG can not be used strictly as a surface probe. Special experimental geometries, e.g. where the surface of the probe is modified by adsorption of different species, allow to distinguish between the surface and bulk contribution to the signal.

In a thin film geometry, where multiple reflections of both the fundamental and the second harmonic beams occur inside the film (Fig.2.7), $(\delta\text{-}\beta\text{-}2\gamma)(\boldsymbol{E}\cdot\nabla)E_i \neq 0$. In this case, the total SH field generated by the nonlinear film is a vectorial sum of the SH field generated in the bulk of the film ($\boldsymbol{E}^B(\Omega)$), the field generated at the surface ($\boldsymbol{E}^S(\Omega)$), and the field generated at the interface with the substrate ($\boldsymbol{E}^I(\Omega)$) [KJJ93, Koo93, WJS95]:

$$\boldsymbol{E}(\Omega) = \boldsymbol{E}^B(\Omega) + \boldsymbol{E}^S(\Omega) + \boldsymbol{E}^I(\Omega) \,, \tag{2.6}$$

with a total SH output

$$S(\Omega) = \frac{8\pi^3\Omega^2}{\hbar c^3}\sec^2\theta_\Omega\left|\chi^{(2)}_{eff}\right|^2 I^2(\omega)\cdot A\cdot T \,. \tag{2.7}$$

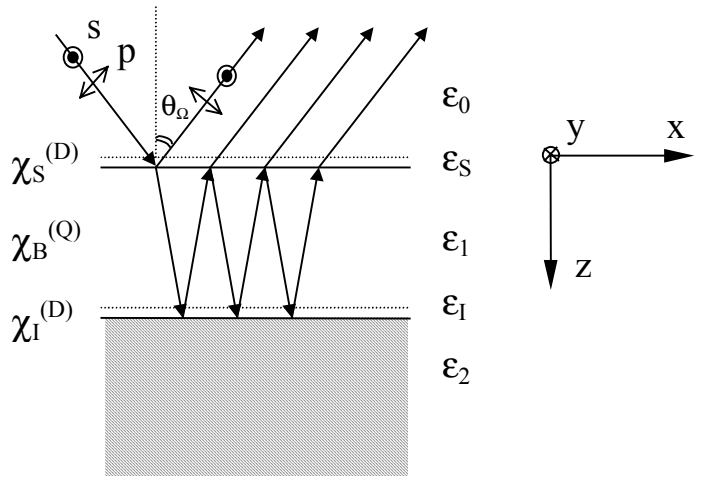


*Fig.2.7. SHG in a thin film geometry, with multiple reflections of both the fundamental and the second harmonic beams inside the film.*

The effective susceptibility tensor is given by

$$\begin{aligned}\chi^{(2)}_{eff} &= \hat{e}(\Omega)\cdot\vec{L}(\Omega,z=0):\vec{\chi}^{(2)}_S:\vec{L}(\omega,z=0)\hat{e}(\omega)\vec{L}(\omega,z=0)\hat{e}(\omega)\\ &+\hat{e}(\Omega)\vec{L}(\Omega,z=d):\vec{\chi}^{(2)}_I:\vec{L}(\omega,z=d)\hat{e}(\omega)\vec{L}(\omega,z=d)\hat{e}(\omega)\\ &+\int_0^d\hat{e}(\Omega)\vec{L}(\Omega,z'):\vec{\chi}^{(2)}_B:\vec{L}(\omega,z')\hat{e}(\omega)\vec{L}(\omega,z')\hat{e}(\omega)dz'\end{aligned} \,. \tag{2.8}$$

$\theta_\Omega$ is the exit angle, $A$ the beam cross section, $T$ the pulse width, $\hat{e}(\Omega)$ the unit vector of the field at $\Omega$ and $\vec{\vec{L}}(\omega,z)$ is a diagonal tensor describing the field inside the film, with the elements:

$$
\begin{aligned}
L_{xx}(\omega,z) &= t_1^p\,(e^{ik_{fz}z} - r_I^p e^{ik_{fz}(2d-z)})\frac{\cos\theta_f}{\cos\theta_\omega} \\
L_{yy}(\omega,z) &= t_1^s\,(e^{ik_{fz}z} + r_I^s e^{ik_{fz}(2d-z)}) \\
L_{zz}(\omega,z) &= t_1^p\,(e^{ik_{fz}z} + r_I^p e^{ik_{fz}(2d-z)})\frac{\varepsilon_1^{1/2}}{\varepsilon_f^{1/2}}, \qquad t_1^h = \frac{t_S^h}{1 - r_S^h r_I^h e^{i2k_{fz}d}}\ .
\end{aligned}
\tag{2.9}
$$

$t_S^h$, $r_S^h$ and $r_I^h$ (with $h$ defining the polarisation, $s$ or $p$) are the Fresnel transmission and reflection coefficients at the surface and the film-substrate interface, respectively. Because of the phase factors in $\vec{\vec{L}}$, the bulk term in $\chi_{eff}^{(2)}$ will exhibit a composite interference pattern as the thickness d varies. The interface, surface and bulk term can have relative phase differences and their interference also changes with $d$.

| component | s-p | p-p | m-s |
|---|---|---|---|
| $\delta$ - $\beta$ - $2\gamma$ | | • | • |
| $\chi^D_{s,yzy}$ | | • | • |
| $\chi^D_{I,yzy}$ | | • | • |
| $\chi^D_{s,zyy}$ - $\gamma$ | • | • | |
| $\chi^D_{I,zyy}$ + $\gamma$ | • | • | |
| $\chi^D_{s,zzz}$ - $\gamma$ | | • | |
| $\chi^D_{I,zzz}$ + $\gamma$ | | • | |

*Table2.1. Nonlinear susceptibilities probed for various polarisation combinations from a thin film*

The nonvanishing independent susceptibility elements are listed in Table 2.1 [Koo93, WJS95]. Only some of these elements will contribute to the generated SH field when different polarisations for the input and the output fields are chosen. The three polarisation combinations used in our measurements are listed in the table: the p-polarised SH generated either by a p-polarised fundamental (labelled p-p) or by a s-polarised fundamental (labelled s-p) and the s-polarised SH generated by a fundamental polarised at an angle of 45° from the plane of incidence (labelled m-s; m states for “mixed”).

### 2.3.2 Rotational anisotropy

The anisotropic contribution to the bulk nonlinear polarization for SHG from leading-order nonlocal terms in a homogeneous medium is given by

$$P_i^{anis}(\Omega) = \zeta E_i \nabla_i E_i \,. \tag{2.10}$$

For cubic centrosymmetric materials (as the case for the fcc-crystallised $C_{60}$), $\zeta = \chi^Q_{iiii} - (\chi^Q_{ijji} + \chi^Q_{iijj} + \chi^Q_{ijij}) \neq 0$. In the case of the (111) face of an fcc crystal, having $C_{3v}$ symmetry, the non-vanishing tensor components of the $\chi_s^D$ will be the isotropic elements $\chi^D_{s,yzy}$, $\chi^D_{s,zyy}$, $\chi^D_{s,zzz}$, which were considered in the previous chapter, and an additional anisotropic element $\chi^D_{s,xxx} = -\chi^D_{s,xyy} = -\chi^D_{s,yxy}$. The Cartesian coordinate axes coincide, in this notation, with the principal crystallographic axes. The tensor components need to be transformed into the laboratory coordinates in order to estimate the values of the generated fields in different polarisation combinations.

Sipe et al. [SMD87] derived explicit expressions for the reflected second harmonic and third harmonic fields from (100), (111) and (110) faces of cubic centrosymmetric single crystals, assuming that the surface will exhibit the same symmetry as the underlying bulk material (i.e. an ideal unreconstructed surface). The SH intensity will be strongly modulated as the sample will be rotated about its surface normal. For the (111) orientation, the variation of the SH fields (generated either by a p-polarised or by an s-polarised fundamental) with an arbitrary azimuthal angle can be summarised in a compact form as

$$E_p(\Omega) = a_{hp} + b_{hp} \cdot cos3\psi \tag{2.11}$$

$$E_s(\Omega) = c_{hs} \cdot sin3\psi \,, \tag{2.12}$$

with the polarisation of the input field $h = s$ or $p$. The complex coefficients $b_{hp}$ and $c_{hs}$ depend only on the anisotropic nonlinear coefficients $\zeta$ and $\chi^D_{s,xxx}$, while the complex coefficients $a_{hp}$ include contributions from $\zeta$ and from the nonvanishing isotropic tensor components listed in Table 2.1.

### 2.3.3 Resonant enhancement

A brief look into the microscopic expression for the second-order susceptibility can help understanding the role of resonances for the enhancement of the SH signal. The expression for

the bulk $\chi^{(2)}$ as found within the electric dipole approximation in the density matrix formalism (for a thorough derivation see e.g. Chapter 2 in ref.[She84]) is given here as an example,

$$\chi^{(2)}_{ijk}(-2\omega;\omega,\omega) =$$

$$-\frac{Ne^3}{2\hbar^2} S \sum_{nn'n''} \left[ \frac{\langle n|r_i|n''\rangle\langle n''|r_j|n'\rangle\langle n'|r_k|n\rangle}{(2\omega-\omega_{n''n}+i\Gamma_{n''n})(\omega_{n'n}-\omega+i\Gamma_{n'n})} + \frac{\langle n|r_j|n''\rangle\langle n''|r_k|n'\rangle\langle n'|r_i|n\rangle}{(2\omega+\omega_{n'n}+i\Gamma_{n'n})(\omega+\omega_{n''n}+i\Gamma_{n''n})} - \right.$$

$$\left. - \frac{\langle n|r_k|n''\rangle\langle n''|r_i|n'\rangle\langle n'|r_j|n\rangle}{(2\omega-\omega_{n'n''}+i\Gamma_{n'n''})} \times \left( \frac{1}{\omega+\omega_{n''n}+i\Gamma_{n''n}} + \frac{1}{\omega-\omega_{n'n}+i\Gamma_{n'n}} \right) \right] \rho_n \ , \qquad (2.13)$$

where $N$ is the density of cells in which the localised orbitals are defined, $S$ is a symmetrising operator summing over the permutations $j \leftrightarrow k$, $n$, $n'$ and $n''$ range over the full set of eigenstates of the localised system, $\Gamma_{n'n}$ is the off-diagonal damping system and $\rho_n$ is the Fermi occupation factor [Koo93]. One can see from this expression that, whenever the fundamental or the second harmonic field will be close to a resonance in the system, the SH signal will be enhanced.

The SHG in $C_{60}$ at 1064 nm (1.165 eV) is naturally determined by the optical properties of solid $C_{60}$ at low excitation energies. Vibrational and optical spectroscopic studies have shown that $C_{60}$ forms a highly molecular solid. Its electronic structure in the solid state is therefore closely related to the electronic structure of the isolated molecule. The single-electron diagram of the molecular energy levels with their icosahedral symmetry identifications, as found from Hückel calculations (Chapter 1.7 in ref.[EkR00]) are shown in Fig.2.8a. The electronic levels are first filled according to their orbital angular momentum quantum numbers $\ell$, and then by imposing level splitting in accordance with the icosahedral symmetry of $C_{60}$, treated as a perturbation [DDE96]. 50 out of the 60 $\pi$ electrons of $C_{60}$ fully occupy the angular momentum states through $\ell = 4$. The $\ell = 5$ state splits in icosahedral symmetry into the $h_u + t_{1u} + t_{2u}$ irreducible representations. The level of lowest energy is the fivefold $h_u$ level, which is completely filled with the 10 available electrons.

The electronic transitions between the Highest Occupied Molecular Orbital (HOMO) $h_u$ and the Lowest Unoccupied Molecular Orbital (LUMO) $t_{1u}$ are electrical-dipole (E1) forbidden. However, due to a Herzberg-Teller electron-vibration coupling, E1 transitions become possible between these coupled "vibronic" states of altered symmetry. These transitions can be observed in the optical absorption spectrum of solid $C_{60}$ (Fig.2.8c) and in solutions of $C_{60}$ in hexane (see Chapter 13 in ref.[DDE96]).

Fig.2.8b shows a multi-electron level diagram, for the $h_g^{10}h_u^{10}$ ground level and the $h_g^{10}h_u^{9}t_{1u}^{1}$ exciton configuration. The calculations of Negri et al. [NOZ98] show that this excitonic level is split into $T_{1g}$, $T_{2g}$, $G_g$ and $H_g$ multiplets by symmetry. The excitation $^1A_g \rightarrow {}^1T_{1g}$ is magnetic dipole (M1) allowed, while the excitation $^1A_g \rightarrow {}^1H_g$ is electric quadrupole allowed. The M1 transition has been experimentally established to be at 1.81 eV [KJJ93]. The $^1H_g$ level should lay 0.54 eV higher than the $^1T_{1g}$ level according to the calculations, therefore the electric-quadrupole (E2) allowed transition should be at 2.35 eV.

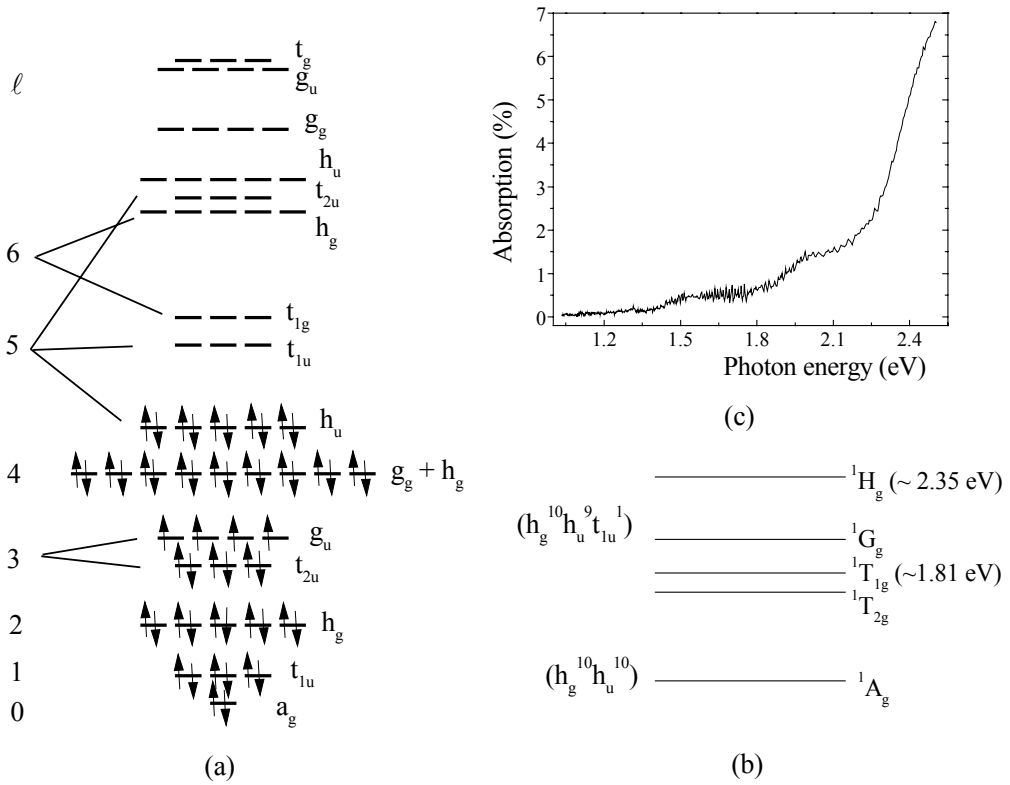


*Fig.2.8. Electronic levels for molecular $C_{60}$: (a) single electron level diagram (Hückel calculations) [DDE96] and (b) the lowest-lying exciton multiplets [WJS95, NOZ98]; the experimentally determined energies are given in parenthesis; (c) absorption spectrum from a $C_{60}$ film in the low-energy region.*

The fundamental laser radiation at $h\nu = 1.165$ eV is far from any resonance in $C_{60}$. The SH output radiation at 2.32 eV, though, is close to the resonance with the $^1H_g$ level. This resonance has E1 character (through the vibronic coupling) in the case of the susceptibility $\vec{\chi}^{P}$, which microscopically is due to transitions of E2 and M1 character in one input field and of E1 character in the other input field and the output field. For the $\vec{\chi}^{Q}$ susceptibility, transitions for both input fields are of E1 character, while for the output field one has E2 character. Therefore, $\vec{\chi}^{Q}$ will be enhanced due to the E2 allowed transition from $^1A_{1g}$ to $^1H_{1g}$ [WJS95]. By measuring

the SHG spectrum from $C_{60}$ films for the fundamental energy range 1.0 – 2.3 eV, Kuhnke et al. [KEK98] have more precisely found this resonance to occur for 1.18 eV fundamental frequency, i.e. the energy of the $^1A_g \rightarrow {}^1H_g$ transition is 2.36 eV.

## 2.4 Experimental setup

### 2.4.1 Measurements under UHV

The SH signal can be affected by any impurity present either in the film or on the surface of the film. Both the reaction kinetics and the nature of the photoreaction are also strongly disturbed by the presence of oxygen in the films. The experiments on photopolymerisation kinetics were therefore conducted under Ultra High Vacuum (UHV) conditions. The UHV system was pumped by turbomolecular pumps and a titanium sublimation pump, giving a base pressure lower than $10^{-10}$ mbar. A Ni(111) single crystal was used as a substrate for the experiments. The Ni(111) substrate was mounted on a manipulator allowing for x,y,z translation, axial and azimuthal rotation. The azimuthal rotation was limited to 270°. The UHV apparatus was equipped with a SPECS IQE 12/38 ion sputter gun and a Perkin Elmer low energy electron diffraction and Auger spectroscopy unit. The crystal was cleaned by cycles of flash-heating (by electron bombardment) up to 900 °C and sputtering with $Ar^+$ ions of 1 keV energy, at a temperature of 500°C. The quality of the surface was checked from LEED patterns and Auger spectra.

Hoechst "gold grade" $C_{60}$ was charged into inert ceramic crucibles and degassed from solvents at 300 °C for a few hours. Any contact of the fullerenes with transition metals that catalyse decomposition was avoided within the evaporator [BET99, EBH99]. The material was sublimated from a Knudsen cell (WA Technology) at 500 °C. The deposition rate was calibrated by monitoring the attenuation of the Auger peak from the Ni substrate at 61 eV as a function of the surface coverage for up to two monolayers of $C_{60}$, as illustrated in Fig.2.9. The curve in the figure is divided into three equally spaced segments. Each segment corresponds to the growth of one $C_{60}$ layer, and the change in slope (occurring in this case at 73 and 146 s, as marked in the figure) determines the completion of the layer [QBW98, SeK93]. This behaviour is consistent with a layer-by-layer growth mode for $C_{60}$ on Ni(111).

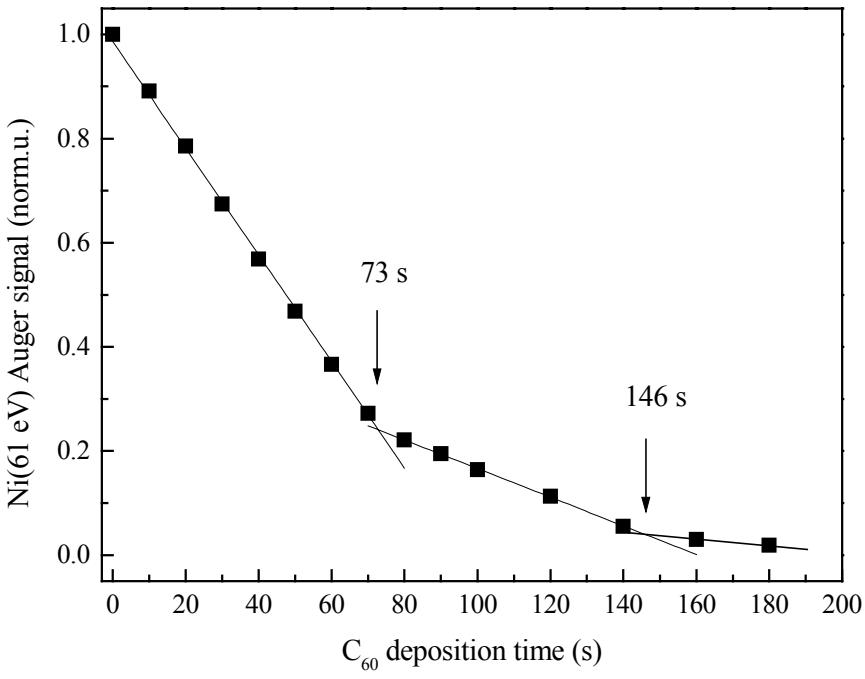


*Fig.2.9. Ni Auger signal versus $C_{60}$ deposition time on Ni(111) at 160 °C.*

The pressure during the deposition was typically lower than $1 \cdot 10^{-9}$ mbar. Since the crystallinity of the films is very important for the topochemistry of the photopolymerisation reaction, we checked a few combinations of deposition rates and substrate temperatures in order to get the best crystallinity of the deposit. The optimal conditions that we found for our deposition geometry were a rate of 1.33 ML/min and a substrate temperature of 160 °C.

The second harmonic generation was measured in reflection geometry. By limitations of the UHV chamber, these measurements were performed at a fixed angle of incidence (45°). The laser system used for these experiments was a BM Industries Nd:YAG laser (Model 502) at 1064 nm, with a pulse width of 30 ps and a repetition rate of 10 Hz. The fluence on the samples was 5-7 mJ/cm$^2$, lower than the damage threshold. No laser-induced changes of the $C_{60}$ sample could be observed, even after hours of irradiation. The optical set-up is shown in Fig.2.10. The SHG was monitored in different polarisation combinations, by using a Glan-laser polariser in combination with a Fresnel rhomb half-wave plate in the input beam, and a Glan-laser polariser in the output beam.

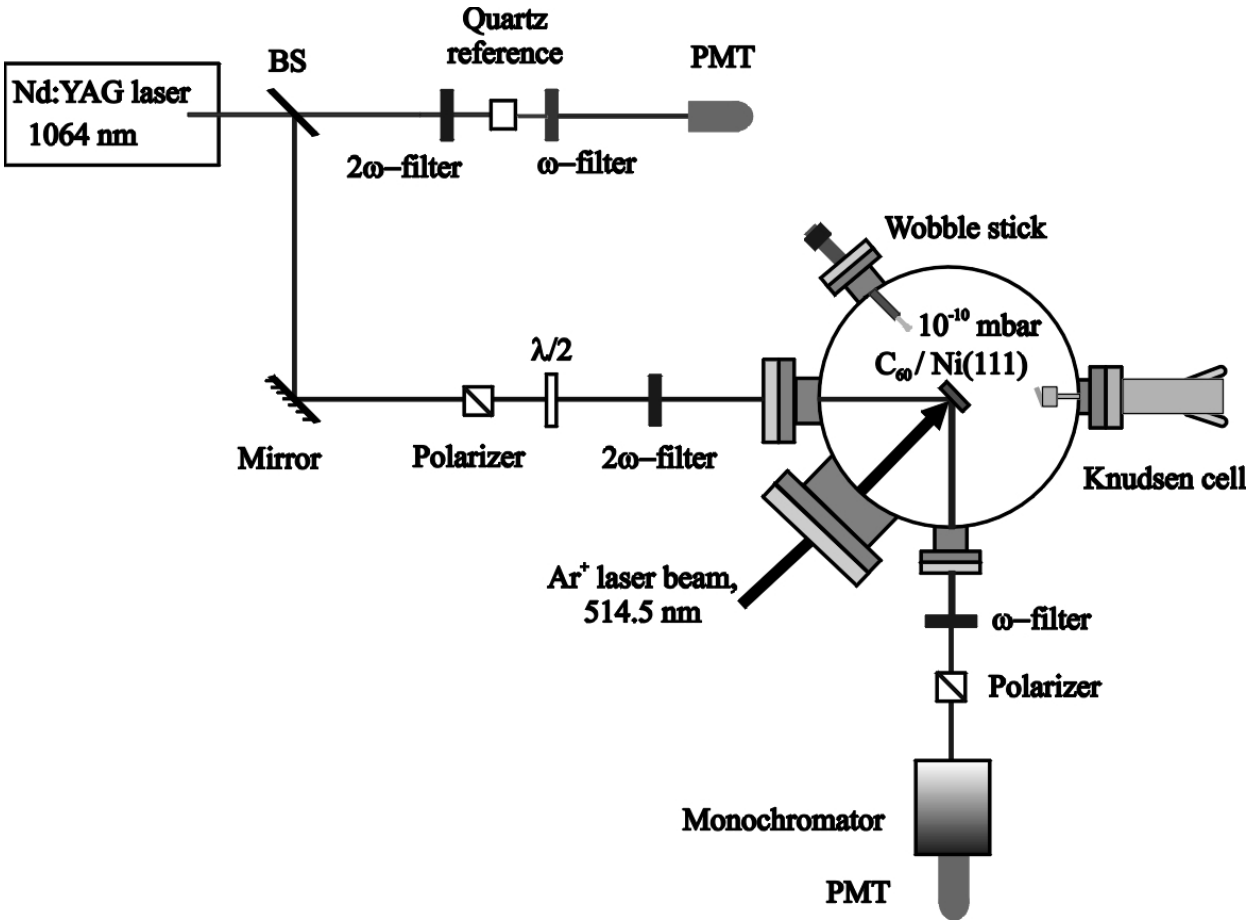


*Fig.2.10. Experimental set-up*

A careful frequency filtering of the light is required both in the input and particularly in the output beam, because of the very low efficiency of the SHG from centrosymmetric media. For $C_{60}$, second harmonic reflectivities of the order of $10^{-24}$ $m^2/W$ (equivalent to $10^{-12}$ for the intensities used here) are expected for the second harmonic generated at 532 nm. It is therefore clear that a discrimination ratio of the order of $10^{15}$ between the fundamental and the second harmonic is necessary for accurate measurements. A set of colour filters was used in the input beam right before the entrance into the UHV chamber for 'cleaning' the fundamental beam at 1064 nm from any residual second harmonic light generated through the optical components in its path. In the output beam, the chromatic filtering was further improved by the use of a monochromator (Jobin Yvon H10-UV) with monochromator slits of 2 mm, giving a spectral resolution of 16 nm. No background light was detected around the 532 nm wavelength (the measurements were performed in a dark room). The second harmonic signal was detected with a Hamamatsu H3177 photomultiplier and recorded via a Stanford Instruments SR250 gated integrator. The instabilities in the laser intensity were compensated by calculating the ratio of

the $C_{60}$ signal with a SH reference signal from a quartz crystal recorded in parallel ($I_{C_{60}}^{SH} / I_{ref}^{SH}$), as shown in Fig.2.10.

The alignment of the surface normal parallel to the rotation axis is crucial for the measurements with azimuthal rotation of the crystal. Any misalignment causes a beam deviation while rotating the sample and adjustments are particularly difficult to make under UHV conditions, which include crystal cleaning procedures at high temperatures. The Ni crystal was fixed with four twisted tantalum wires, shown in Fig.2.11. Two extra bars are placed over these wires, and the four screws holding them can adjust the orientation of the crystal by pressing the bars onto the wires. A pre-alignment of the crystal is made before closing the chamber. An UHV wobbling and rotating stick equipped with a screwdriver head was used to adjust the orientation of the crystal right before the rotational measurement. Any final displacement (of maximum 3 mm at the 2 mm entrance slit of the detection system) was reduced with a focusing lens in front of the monochromator.

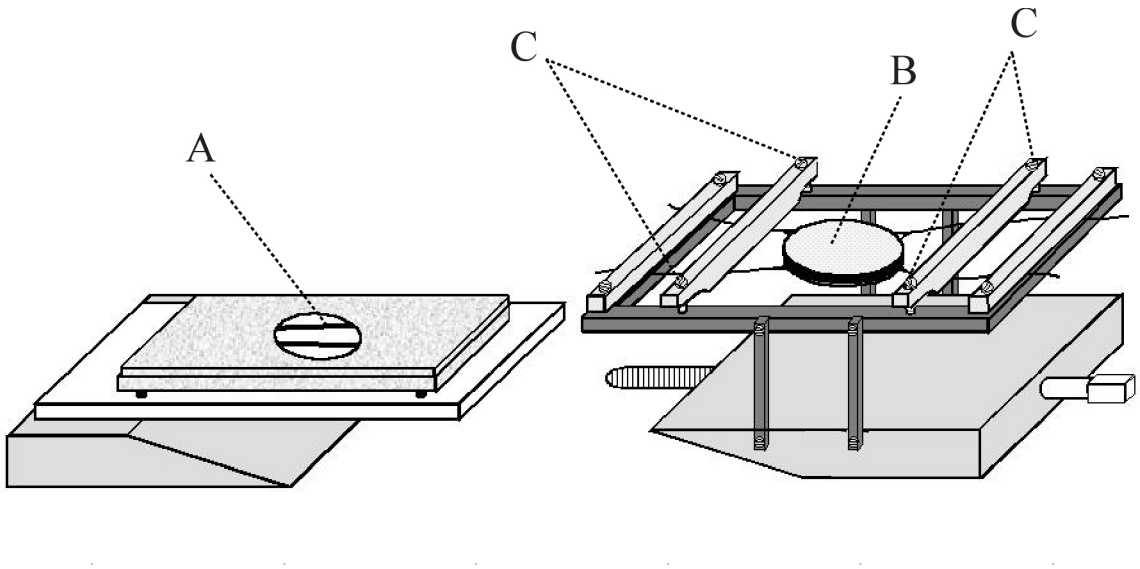


*Fig.2.11. Sample holder: A- heating filament mounted in a molybdenum box with an orifice; B – Ni(111) crystal held by a frame of tantalum wires; C – screws for adjustment of the crystal orientation.*

The $C_{60}$ films were photopolymerised with an $Ar^+$ laser at 514.5 nm guided through an optical fiber, with a fairly homogeneous power density of 320 mW/cm$^2$. The films were irradiated in situ, right after the cooling of the substrate to about room temperature, and the SHG was checked after each step of irradiation. The substrate temperature increased during irradiation by less than 20 °C above room temperature. The $Ar^+$ laser beam diameter on the sample was 8 mm (with a homogeneous intensity distribution), while the diameter of the

Nd:YAG laser was of 4 mm (full-width at half-maximum from the gaussian profile of the beam, measured with a beam profiler), well placed within the $Ar^+$ laser irradiated area. The whole alignment of the SH set-up was performed by means of a He:Ne laser, carefully aligned with the infrared beam outside the chamber.

### 2.4.2 Measurements in air

Spectroscopic evidence of polymerisation after different steps of irradiation was obtained from vibrational infrared (IR) spectroscopy. The films for these measurements were deposited on KBr pellets, in a separated high vacuum (HV) chamber, under a base pressure of $5 \cdot 10^{-6}$ mbar. The thickness of the films was in this case monitored with a quartz microbalance. After deposition, the films were irradiated in situ with an $Ar^+$ laser, under the same conditions used for the UHV measurements. After the irradiation, the films were transported in air to a dry-air purged BIORAD FTS-45A Fourier transform infrared spectrometer. Since the changes in the spectra were usually rather small, we chose a resolution of 2 $cm^{-1}$ and an averaging over 256 scans for each spectrum, giving a good signal to noise ratio in the measurements.

Another set of films was deposited in this HV chamber on quartz and on KBr substrates and kept in air and in darkness for a few weeks. After this time, we checked their phototransformation kinetics with SHG in an optical setup similar to the one described for the UHV measurements, except that the samples were irradiated in air. Infrared spectroscopy was again used to obtain information about the phototransformation products in these films.

## 2.5 Photopolymerisation of oxygen-free $C_{60}$ films

### 2.5.1 Azimuthal anisotropy of crystalline films of $C_{60}$

The low energy electron diffraction (LEED) pattern from a film with a thickness of 100 ML, which was deposited under the conditions described in Section 2.3.1, is shown in Fig.2.12. The film is quite well ordered, with the fcc crystalline structure of $C_{60}$ following the (111) orientation of the Ni substrate. For such thick films the surface charging is expected to strongly affect the pattern, since the solid $C_{60}$ behaves as a semiconductor (with a calculated energy gap of 1.5 eV [SaO91]).

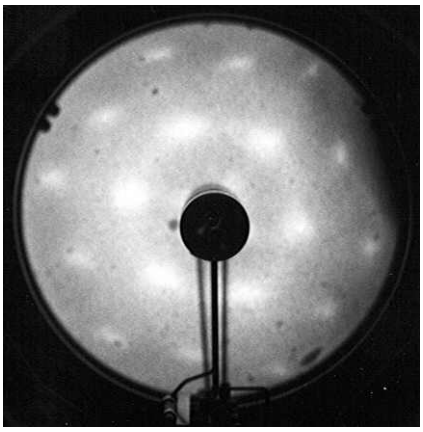

*Fig.2.12*. LEED pattern of a 100 ML $C_{60}$ film

The azimuthal anisotropy of crystalline materials can also be monitored by SHG, as discussed in Section 2.3.2. Fig.2.13 shows the dependence of the SH signal on the azimuthal rotation of this sample, in reflection geometry at 45° angle of incidence. The two input-output polarisation combinations (p-p and s-p) shown in this picture were also chosen to monitor the kinetics of the photopolymerisation (see discussion in the following section), due to their higher SH efficiency.

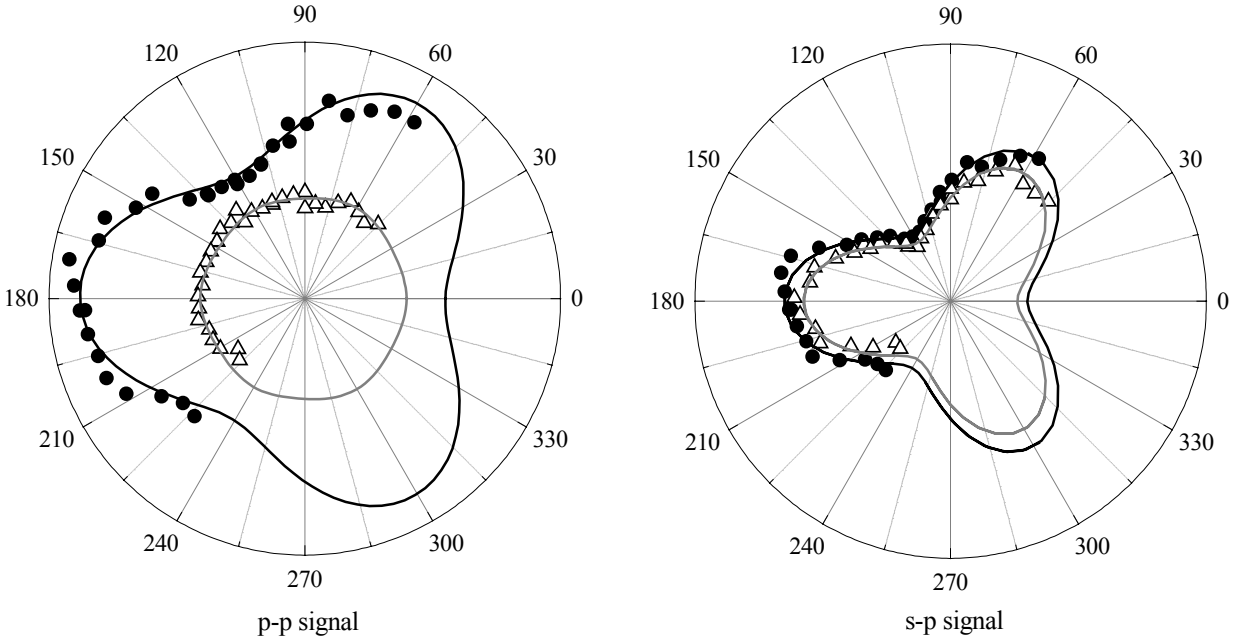


*Fig.2.13. Rotational anisotropy of the SH signal measured in p-p and s-p polarisation combinations. Full circles are the data taken from the pristine film, open triangles after irradiation of this film with 1 x $10^{21}$ photons/cm$^2$.*

The anisotropy measured for the pristine $C_{60}$ film is shown with full circle symbols. The film was irradiated for 25 minutes at 320 mW/cm$^2$, an equivalent of $10^{21}$ photons/cm$^2$ and the SH data measured on the irradiated film are given with open triangles. The corresponding lines are

the best fits to the data. We used equation (2.11) to obtain the following formula for fitting the data:

$$I_{SH} = \left| a \cdot e^{-i\varphi} + b \cdot \cos 3\psi \right|^2 , \qquad (2.14)$$

where a phase difference $e^{-i\varphi}$ between the isotropic and the anisotropic terms was included to account for the fact that *a* and *b* are complex coefficients. The results of the fits are presented in Table 2.2; parameters *a* and *b* are given in arbitrary units.

| Polarisation combination | Isotropic term (*a*) | | Anisotropic term (*b*) | | Phase difference ($\varphi$) | |
|---|---|---|---|---|---|---|
| | pristine | polymerised | pristine | polymerised | pristine | polymerised |
| s-p | 1.79 | 1.67 | 0.70 | 0.69 | 90 | 90 |
| p-p | 2.22 | 1.66 | 0.26 | 0.25 | 179 | 93 |
| m-s | 1.44 | 0.55 | 0.20 | 0,18 | 140 | 104 |

*Table 2.2. Fit parameters of the azimuthal scans in Fig.2.13.*

The change in the s-p signal can be described by a lowering of the isotropic contribution. The change in the p-p signal shows a strong decrease of the isotropic term and a phase shift between the isotropic and the anisotropic component. The anisotropic part of the signals is barely affected by the laser irradiation.

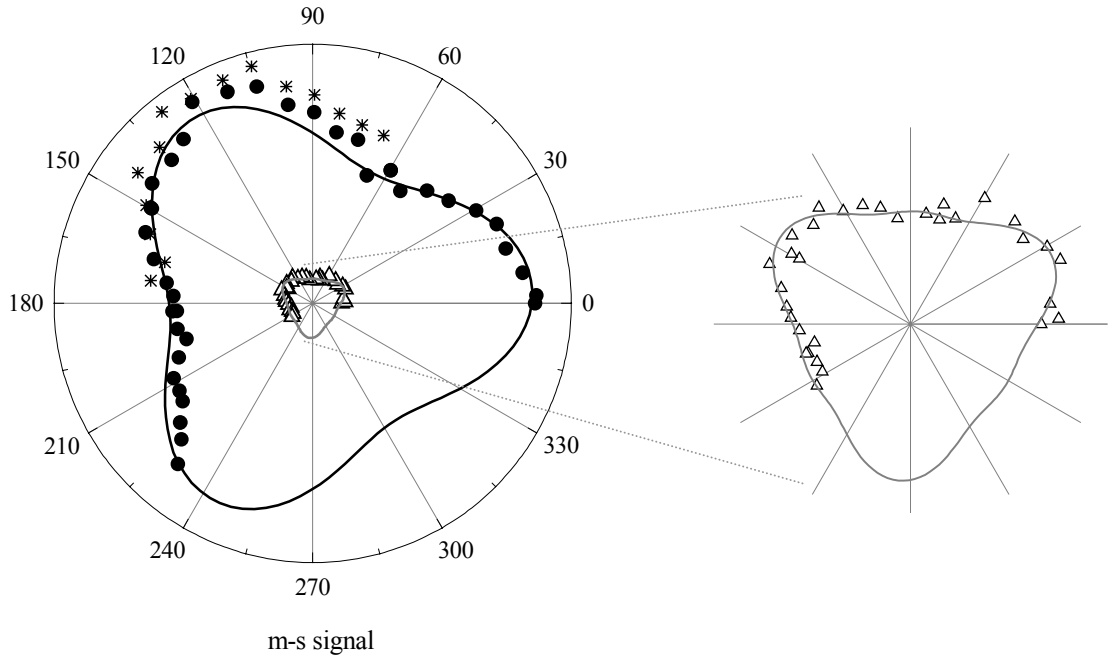


*Fig.2.14. Anisotropy of the SH signal measured in m-s polarisation combination. Full circles: data taken from the pristine film, open triangles: after irradiation of this film with 1 x $10^{21}$ photons/cm$^2$ (graph magnified in the right part of the figure); stars: after heating of the polymerised film for one hour at 200 °C.*

The s-polarised signal generated by a mixed-polarised fundamental (i.e. the polarisation angle is 45° from the plane of incidence) in Fig.2.14 also shows the decrease in the anisotropic term and the phase shift between the isotropic and anisotropic components, together with a shift of 22° in the anisotropic pattern. This shift is only observed for this polarisation combination and it can not be explained from our qualitative analysis of these measurements. Thermal heating of the samples for one hour at 200 °C showed a full recovery of the SHG to the level of the not irradiated film (data marked with stars in Fig.2.14). This is in good agreement with previously reported Raman measurements [WHB94, SIN01] in which thermally activated breaking of the $C_{60}$ polymer bonds was observed.

Hassanien et al. [HGD97] observed in an atomic force microscopy that the intermolecular distance between the $C_{60}$ molecules in the films was reduced from an initial measured value of 10.5 ± 0.1 Å, as in the fcc crystal, to 9.2 ± 0.1 Å, after a few hours of irradiation with an $Ar^+$ laser at 514.5 nm, with power densities of 5 - 26 W/cm$^2$. In the first paper on the photopolymerisation of $C_{60}$, Rao et al. [RZW93] found a broadening of 20% in the X-ray diffraction (XRD) pattern of these films. In a more recent XRD study on crystalline powder of $C_{60}$ irradiated for three weeks with a xenon lamp, Pusztai et al. [POF99] concluded that the crystalline structure of $C_{60}$ remains face centered cubic with a 0.25 Å contraction of the lattice. The large width of the new XRD peaks indicated that the polymerisation builds up small closed oligomers. The results we obtain here from the anisotropy of the SHG signal are indicating that the crystalline structure of the films is not dramatically affected after the low irradiation doses used in our experiments. The first stages of the photopolymerisation have, however, a strong influence on the magnitude and (relative) phase of the isotropic second-order nonlinear response of the films.

## 2.5.2 Kinetics of photopolymerisation

The photopolymerisation of $C_{60}$ films at low irradiation doses induces only minor changes in the dipole allowed transitions, which manifest as a broadening and a small blue shift of the optical absorption peaks. Those spectral modifications are typically measured after irradiation doses for polymerisation that are a few orders of magnitude higher (e.g. 80 W/cm$^2$ at 488 nm for 60 min in ref. [MOY97]) compared to the doses used in our work. The measurements of the SHG signal as a function of the $Ar^+$ laser irradiation time are shown in Fig.2.15. Each point was averaged over 500 laser shots and the statistical errors are plotted here as error bars. The second harmonic generation was measured as a function of the $Ar^+$ laser irradiation time, converted here

to photons per $cm^2$ in order to account for small laser intensity differences. The data are normalised to the SH signal of the not irradiated sample. We measured the p-polarised second harmonic generated by an s-polarised or p-polarised fundamental. The measurements show a decrease of the SH signal in the p-p polarization combination. An initial increase for the s-p signal forming a maximum at $1.4 \cdot 10^{20}$ photons/$cm^2$ is indicating a double exponential behaviour.

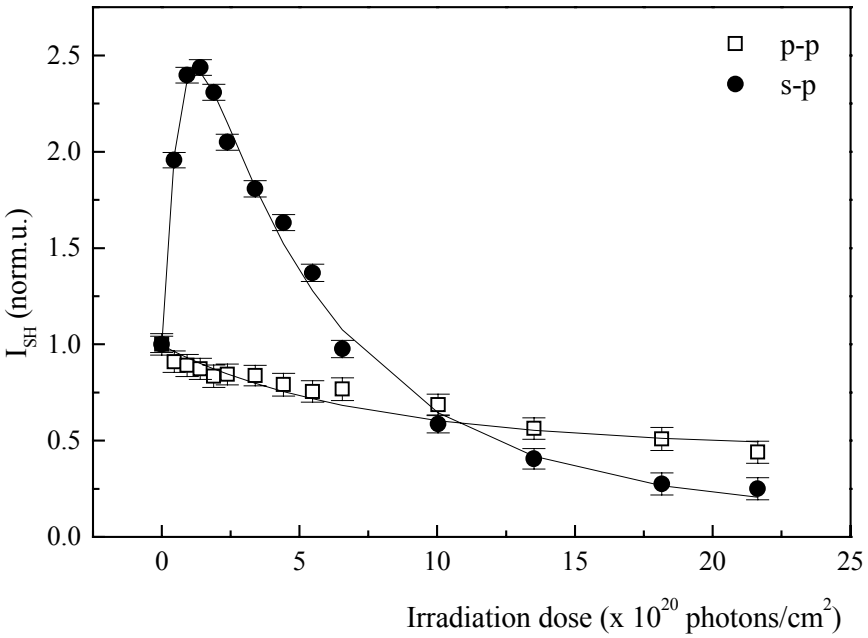


*Fig.2.15. Normalised second harmonic signal as a function of irradiation doses for an oxygen-free $C_{60}$ film of 650 nm: p-polarised signal generated by an s-polarised (s-p) or p-polarised (p-p) fundamental.*

The data were fitted with the following expression:

$$I_{2\omega} = \left| a_{sp/pp} \cdot e^{-d/\delta_1} + b_{sp/pp} \cdot e^{-d/\delta_2} + c_{sp/pp} \right|^2 \cdot I_{\omega}^2 , \qquad (2.15)$$

where $a_{sp}$, $b_{sp}$, $c_{sp}$, $a_{pp}$, $b_{pp}$, and $c_{pp}$ are complex coefficients describing the second harmonic generation efficiency of the system under transformation in the corresponding polarisation combination, and relative to the efficiency of the pristine material. These coefficients probe different nonlinear optical constants depending on the corresponding polarization combination and they can have different signs, due to their relative phases. The values obtained from the double exponential fit for the $\delta_1$ and $\delta_2$ constants are

$\delta_1 = (0.5 \cdot \pm\, 0.3)$ x $10^{20}$ photons/$cm^2$

$\delta_2 = (8.7 \pm 4)$ x $10^{20}$ photons/$cm^2$ .

The exponential behaviour is the same for both s-p and p-p polarization combinations and reflects the transformation kinetics of the film by irradiation. The maximum in the evolution of the s-p signal is expressed by a different sign of $a_{sp}$, relative to the $b_{sp}$ and $c_{sp}$ coefficients. The signal saturates at a level of 46% for the p-p signal and 11% in the case of the s-p polarization combination. No change in the SH signal was observed due to the irradiation of the film with the Nd-YAG laser.

SHG is very sensitive to changes in the local fields, as well as to the phase coherence between the radiating states located on different molecules [JEK95]. In Kuhnke et al. [KBB96], the photoexcitation of one $C_{60}$ molecule out of 1000 was shown to quench the SH signal by one order of magnitude. Therefore, it is understandable that a low concentration of dimers and oligomers in our films can significantly change the SH signal. We consider two main processes to be responsible for the change in the SH signal: the formation of $C_{60}$ dimers and the formation of oligomers, initially trimers, through the loss of dimers and monomers. While the first dose constant $\delta_1$ is interpreted by a majority formation of dimers (over oligomers) modifying the SH intensity, $\delta_2$ is determined by a predominance of oligomers (over dimers) in the film, which is evidenced with IR spectroscopy (see Section 2.4.3 for details). After a certain concentration of higher oligomers is formed in the film, no further conversion can be monitored by SHG.

The Raman spectra measured in air on a film polymerised under UHV with a dose of $10^{21}$ photons/cm$^2$ showed the typical softening of the $A_g(2)$ pinching mode from 1469 cm$^{-1}$ to 1459 cm$^{-1}$. When trying to dissolve the film in toluene, the area exposed to the laser beam remained on the substrate, which confirms that the material was already polymerised after these low irradiation doses.

### 2.5.3 IR spectroscopy

Films of 650 nm thickness were deposited under similar conditions compared to the films studied by SHG, in a high vacuum chamber on KBr substrates. After the deposition of the films and the cooling of the substrates, the samples were irradiated in situ with an $Ar^+$ laser at 514.5 nm and 320 mW/cm$^2$ for 1 or 20 minutes. The irradiation times were chosen to correspond to the photon doses constants of the exponential changes in the SH signal (0.5 and $8.7 \cdot 10^{20}$ photons/cm$^2$, respectively). The films were then transported in air to the FTIR spectrometer. The spectrum of the pristine $C_{60}$ is shown in Fig.2.16. It consists of four prominent lines at 526, 576, 1183 and 1429 cm$^{-1}$, which are the only first-order infrared-active modes of the $C_{60}$ molecule, identically found for the weakly bonded molecular solid. The weaker features at 712, 738, 775,

962, 1100, 1259 $cm^{-1}$, indicated in the figure, correspond to second-order combination modes [DDE96].

Since the changes induced on the IR spectra by the low irradiation doses used in our experiment are small, the spectrum of the pristine part of each film was subtracted from the spectrum of the irradiated part. The difference spectra, thus calculated, are presented in Fig.2.17. An onset of the polymerisation after only one minute of irradiation (0.5 x $10^{20}$ photons/$cm^2$) can be observed. The absorbance corresponding to the $F_{1u}$ modes of pristine $C_{60}$ at 526, 575, 1183 and 1429 $cm^{-1}$, seen as negative peaks in the difference spectra, is strongly decreased, indicating that a very strong loss of monomers occurs after low doses of irradiation. Second-order modes of the pristine $C_{60}$ (1100, 1259, 1290 and 1308 $cm^{-1}$) are also observed to decrease in intensity and continue to decrease with irradiation time

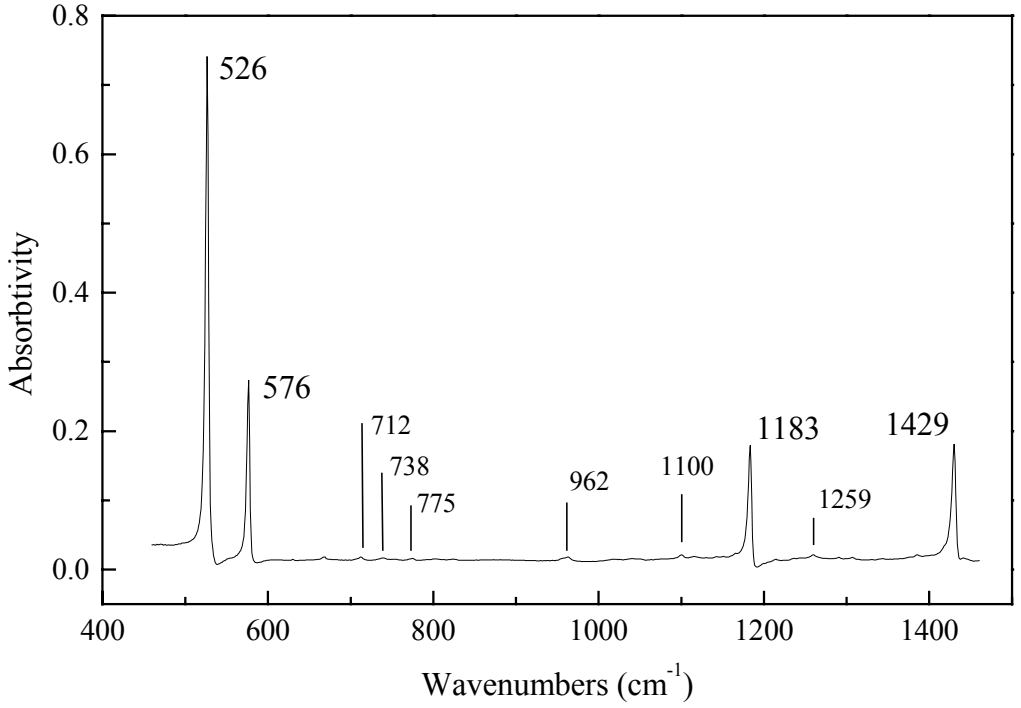


*Fig.2.16. IR spectrum of a pristine $C_{60}$ film*

Three new modes (with positive peaks), at 478, 524 and 746 $cm^{-1}$ are identified and assigned to the $C_{60}$ dimer. This assignment is based on the calculations of V. C. Long et al [LMK00] for the 524 $cm^{-1}$ mode and on the spectra measured by B. Ma et al [MMS98] on purified dimeric $C_{60}$ produced in a mechanochemical reaction. The peak at 524 $cm^{-1}$ is clearly stronger for the one-minute irradiated film, while the other two modes seem to have a similar intensity for the longer irradiation time.

The peaks arising from superposition of dimeric and polymeric modes (549, 660, 667, 732, 706, 762 $cm^{-1}$) and from pure polymeric modes (543, 560, 769, 795, 1227 $cm^{-1}$) [RZW93, MMS98, OnT96] are present in both spectra and increase in intensity with irradiation time. The presence of polymer modes at very low irradiation doses is suggesting a growth around nucleation centers which refer to the small closed oligomeric structures described in the X-ray diffraction work of T. Pusztai et al. [POF99]. The relative amounts of monomeric, dimeric and polymeric species at a certain irradiation time are not estimated since the assignment and relative intensity of corresponding modes are not known. By increasing the number of photons incident on the surface, the amount of dimers tends slightly to decrease, while the polymers increase. The film irradiated with 0.5 x $10^{20}$ photons/$cm^2$ did dissolve in toluene, but significantly slower than the not irradiated film. The film irradiated with $8.7 \cdot 10^{20}$ photons/$cm^2$ did not dissolve within several days.

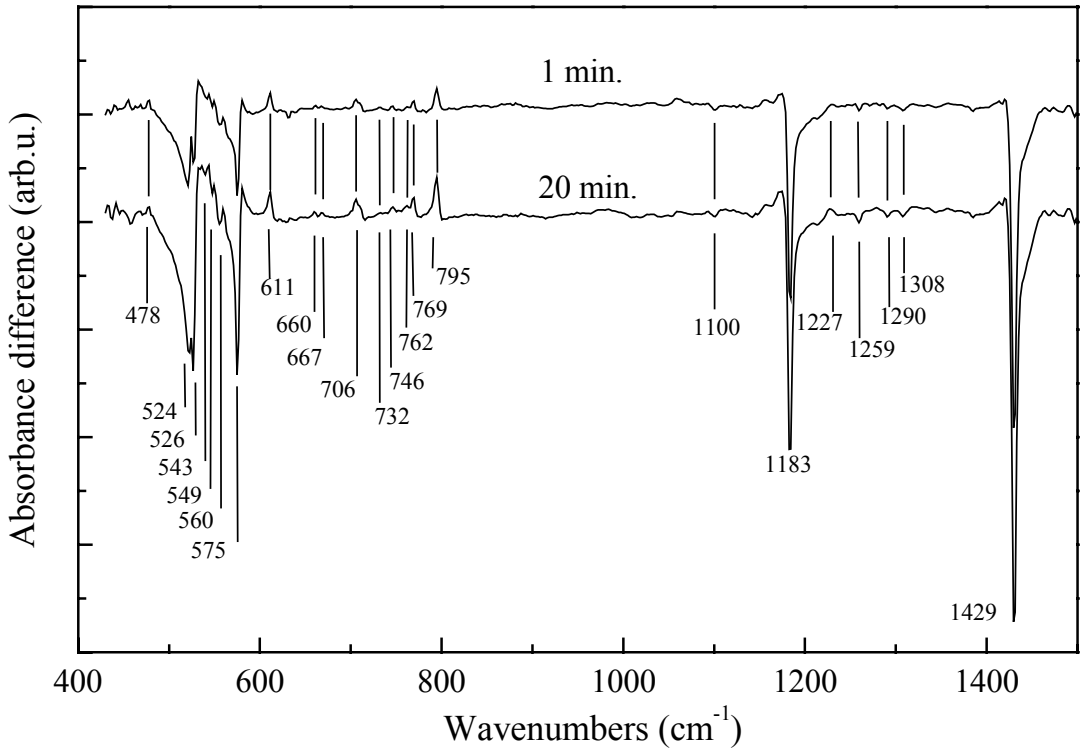


*Fig.2.17. Difference IR absorbance spectra of 650 ML $C_{60}$ films irradiated in situ for one minute and 20 minutes at 320 mW/$cm^2$, respectively.*

S. Park et al [PHK98] showed that the relative amount of dimers and higher oligomers formed at room temperature under UHV conditions in the film equilibrates after about 10 minutes of irradiation with 1200 W/$cm^2$ (~$10^{24}$ photons/$cm^2$). This dose is four orders of magnitude higher compared to our experiments, which show significant photopolymerisation already after an irradiation with $d = 0.5 \cdot 10^{20}$ photons/$cm^2$. With an absorption coefficient $\alpha$ =

2.14 $\mu m^{-1}$ [RWR91] at 514.5 nm and taking into account the molecular density of solid $C_{60}$ $\rho = 1.44 \cdot 10^{21}$ $cm^{-3}$, this corresponds to $N_{abs} = d \cdot \alpha / \rho \sim 740$ photons absorbed per $C_{60}$ molecule. The high number of photons that is necessary to achieve the polymerisation rules out the photodimerisation mechanism proposed in [WHD93], where the absorption rate was considered to be the reaction-limiting rate, with one absorbed photon creating one dimer.

### 2.5.4 Thickness dependence

The kinetics of the phototransformation was studied for different film thickness. Fig.2.18 shows the evolution of the p-p SH signal (normalised to the initial SH yield, before irradiation) for films of 100, 50, 20 and 10 ML, as a function of the irradiation dose.

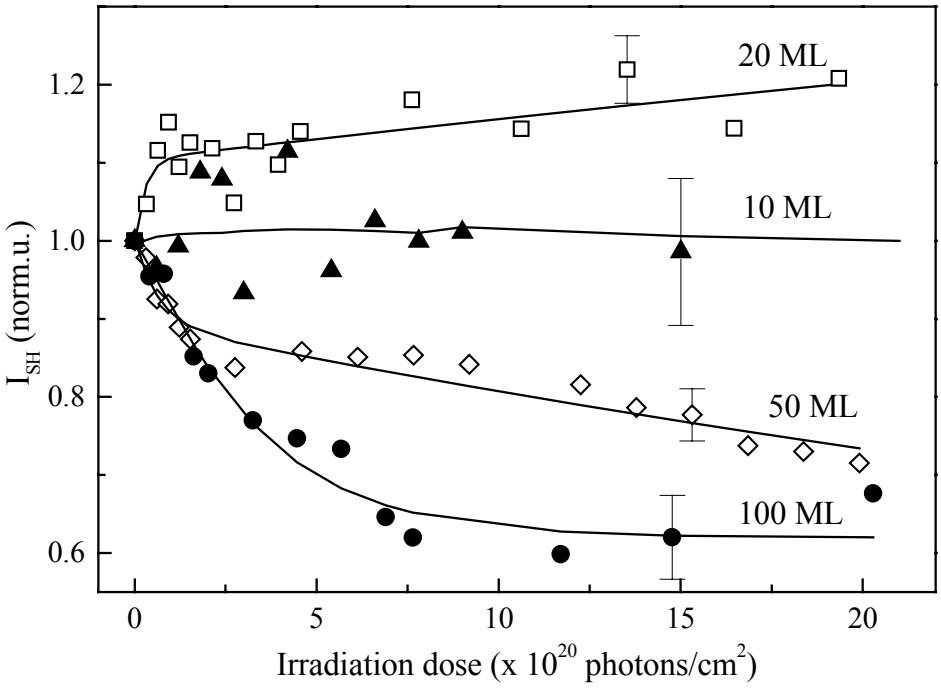


*Fig.2.18. Normalised second harmonic signal as a function of irradiation doses for $C_{60}$ films of different thickness (p-p polarisation combination). For convenience, the level of the error bars is shown only on one point for each series.*

The curves were fitted using the double exponential function given by equation (2.15), and the exponential constants obtained from these fits are given in Table 2.3. The apparent difference in the behaviour of the 20 ML film can be explained by a change of sign in the $c_{pp}$ coefficient relative to the $a_{pp}$ and $b_{pp}$ coefficients and is probably an interference effect. The second exponential constant is increasing by decreasing the film thickness, showing that the reaction is gradually hindered as we approach the substrate.

| | Film thickness | | | |
|---|---|---|---|---|
| | 100 ML | 50 ML | 20 ML | 10 ML |
| $\delta_1$ ($\cdot 10^{20}$ photons/cm$^2$) | 0.8 | 0.6 | 0.3 | > 1000 |
| $\delta_2$ ($\cdot 10^{20}$ photons/cm$^2$) | 5.3 | 82 | 98 | > 1000 |

*Table 2.3. Exponential constants of the double exponential photoinduced changes in the SH signal (p-p polarisation combination) from $C_{60}$ films of 100, 50, 20 and 10 ML thickness.*

For films of 10 ML thickness the SH signal stays at a constant level (within the error bars) and the reaction seems to be suppressed. We have also analysed the changes in the IR spectra of thin films induced by irradiation, in order to confirm that the photopolymerisation reaction is indeed suppressed. Films of 10 ML and 20 ML were deposited on CsI single crystals with smooth surfaces. Two samples were prepared for each film thickness, and one of the samples was irradiated in situ with $2 \cdot 10^{21}$ photons/cm$^2$. The difference absorption spectra between the irradiated and pristine films are presented in Fig.2.19. The total amount of $C_{60}$ material is very low in these very thin films, so that the polymeric modes, with very low intensity, can not be observed from these spectra. The modulated background in the difference spectra is caused by small differences in the quality of the 2 mm thick CsI substrates. However, the most prominent change in the irradiated spectra, the decrease in the intensity of the pristine modes (see also Section 2.5.3 and Fig.2.17), is observed from the film of 20 ML. The positions of these negative peaks, at 526, 576, 1182 and 1429 cm$^{-1}$, are indicated with dotted lines in the figure. The peaks are decreased by about 30% in the 20 ML film. A decrease of these modes was not observed from the 10 ML thick film. It is important to note that changes of ~ 5% in the intensity of the peaks from the 10 ML films should still be detectable from the background noise level. Therefore, we conclude that no transformation of the 10 ML film occurs due to irradiation with the $Ar^+$ laser. This is in good agreement with the Raman measurements performed by Park et al. [PHK98] under UHV conditions, where an onset of the photopolymerisation with film thickness of 15 ML was shown. This thickness threshold was similar for samples irradiated at different temperatures (room temperature, 100 and 150 °C). No conclusive discussion of this threshold behaviour has been given in the literature.

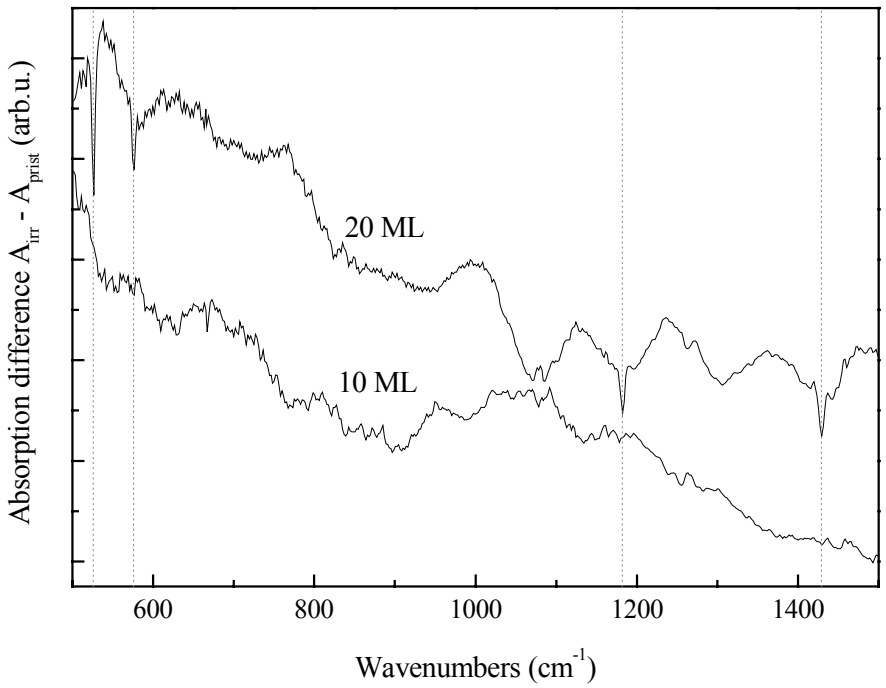


*Fig.2.19. Difference IR absorption spectra of $C_{60}$ films of 10 ML and 20 ML irradiated in situ with $2 \cdot 10^{21}$ photons/$cm^2$. The positions of the $F_{1u}$ modes of $C_{60}$ are marked by dotted lines.*

We refer here to the mechanism of the photopolymerisation described in Section 2.1.3, which involves the self-trapping of the charge transfer excitons as promoters of the polymerisation, to explain this behaviour in the proximity of the substrate. Within this model, the molecules have to remain in the self-trapped CT excitonic state for enough time so that the two molecules involved in the dimerisation process can rotate to the orientation which is necessary for the reaction, i.e. with two double bonds parallel to each other. Therefore, the relaxation dynamics of photoexcitations in thin $C_{60}$ films should be discussed. In a series of articles published in 1996-1997 [KBK96, KBK97, KBE97], Kuhnke et al. showed that the lifetime of photoexcitations in $C_{60}$ (tentatively attributed to Frenkel excitons) decreases dramatically in the proximity of the substrate. We are using the results from a more recent work from Ichida et al. [INS98] on relaxation dynamics in $C_{60}$ films to re- interpret Kuhnke et al. in a way that actually the CT excitons, relevant to the photopolymerisation process, have a reduced lifetime in the proximity of the substrate. These two studies are discussed in more detail below.

Kuhnke et al. [KBB96] have studied the transient SH generated from $C_{60}$ single crystals at 1.165 eV fundamental frequency, either in transmission or in reflection geometry. When pumping the $C_{60}$ with photons of 3.49 eV energy, the SH signal was suppressed by one order of magnitude compared to the signal obtained from the not excited crystal. The same result was

obtained for films of $C_{60}$ on quartz, with a thickness higher that 100 ML [KBK96]. The quenching of the nonlinear response is faster than 45 ps and persists for a time longer than 20 ns (Fig.2.20a) but shorter than 50 ms, which was the repetition time of the laser.

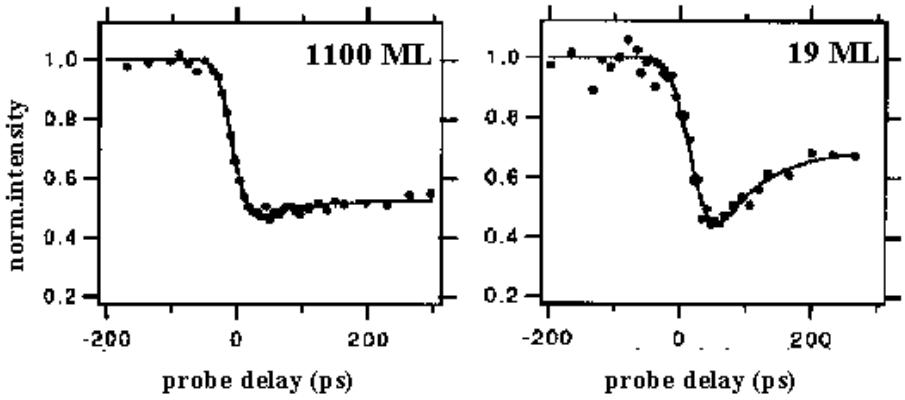


*Fig.2.20. Pump (at 3.49 eV) and SH probe transients in $C_{60}$ films of 1100 and 19 ML on amorphous quartz substrates [KBK96]*

A faster decay of 70 ps becomes prominent for films with a thickness lower than 100 ML (see Fig.2.20b) [KBK96]. This faster decay was ascribed to the coupling to the quartz substrate, inducing the reduction of the exciton lifetime at the interface. By using metal-alkanethiol-$C_{60}$ sandwich structures, the lifetime of the exciton in the proximity of a gold substrate was found to increase with $d^3$ and with $d^4$ for silver, with $d$ the distance from the $C_{60}$ layer to the substrate [KBK97, KBE97]. For a distance of 1 nm from the Au substrate, the lifetime is 44 ps.

The quenching of the SH signal was interpreted as being induced both by singlet and triplet excited states in the $C_{60}$ molecules, implying that the lifetime of Frenkel excitons was monitored in these measurements. In view of a more recent study from Ichida et al. [INS98] on relaxation dynamics in $C_{60}$ films, we can demonstrate that the charge transfer excitons were actually monitored in this study, by comparing the lifetime of the excitation and the energy of the SH photons used as a probe in the measurements of Kuhnke et al.

An extended study of the relaxation dynamics was reported by Ichida et al. [INS98], using transient absorption spectroscopy in the spectral region 1.25 - 3.1 eV over a vast time domain from 100 fs to 100 ms. $C_{60}$ thin films of 150 ML were excited with 3 eV photons and the measurements were performed at a temperature of 80 K. Fig.2.21 shows the differential absorption spectra in the picoseconds (a) and in the milliseconds (b) time region reported in [INS98]. The induced absorption band below 2.4 eV was associated with the transition from the LUMO $t_{1u}$ band to higher conduction bands, by comparison to the induced absorption in solutions of $C_{60}$ in toluene. The lifetime of this induced absorption, attributed to singlet Frenkel

excitons, was estimated to be ~ 400 ps. The transient absorption characteristics of the intramolecular triplet state (increased absorption around 1.65 eV) has only been detected in solutions, while for the solid $C_{60}$ it is not observed, indicating that the intramolecular inter-system crossing does not occur in the $C_{60}$ solid state.

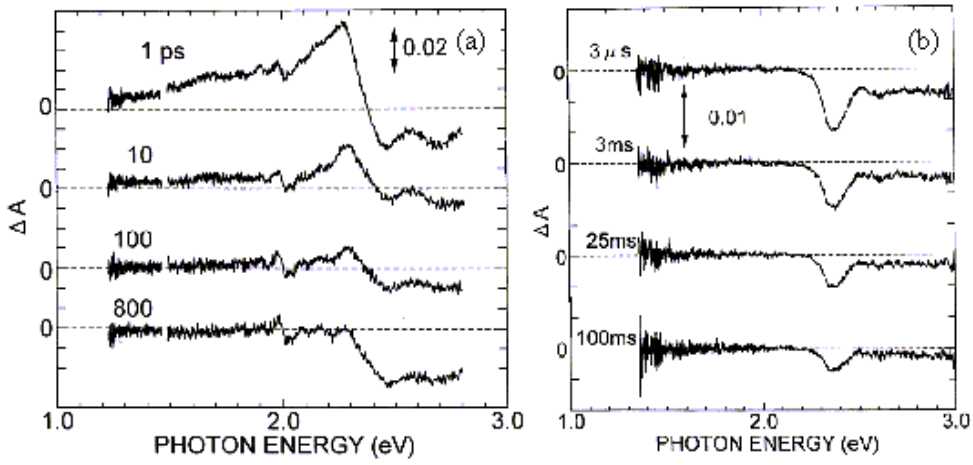


*Fig.2.21.Transient differential absorption spectra of $C_{60}$ thin films at 80 K, following the excitation with 3 eV photons [INS98]*

The decrease of the absorption above 2.4 eV is composed of two bleaching peaks at 2.46 and 2.7 eV and indicates a bleaching of the CT excitons band. In the ms timescale, the bleaching peak at 2.46 eV shifts to 2.37 eV and is attributed to an "intermolecular" triplet state of the CT excitons. The relaxation dynamics proposed for the CT excitons has three main components: a fast relaxation, within 1.3 ps, into a singlet self-trapped CT state; this state has a lifetime of 1.8 ns (also found from luminescence experiments) and will relax to the triplet state of the self-trapped CT exciton via three possible paths: radiative recombination, thermally activated nonradiative recombination through a barrier and intersystem crossing. The triplet state of the self-trapped CT exciton has a lifetime of ~ 50 ms at 80 K. The lifetime of the excitation probed by SHG in the experiments of Kuhnke et al. was "longer than 20 ns". This is much longer than the 400 ps relaxation time measured for the Frenkel excitons by Ichida et al. Therefore, we believe that the SH change is probing the self-trapped states of the CT excitons. The lower lifetime of the SH quenching (lower than 20 ms, since after 50 ms the signal was fully recovered) compared to the lifetime of 50 ms found for the triplet self-trapped CT excitons can be due to the difference in the sample temperature in the two experiments (room temperature and 80 K, respectively). Moreover, the SH generated by the Nd:YAG laser at 1.16 eV is enhanced due to a resonance in the second harmonic frequency at 2.32 eV (see Section 2.3.3). This energy is close to the bleached absorption peaks corresponding to CT excitonic bands, as

discussed above. When probing the excitation by the second harmonics generated with 1.82 eV and 2.02 eV, no change in the signal was observed [KEK98]. This is more evidence that the formation of charge transfer excitons, and not Frenkel excitons, is responsible for the change in the SH signal

The important conclusion of these two correlated studies is that in the proximity of the substrate, the self-trapped state of the charge transfer excitons is rapidly quenched.

The $C_{60}$ molecules are freely spinning about their fcc lattice positions above the orientational ordering temperature of 260 K. The rotational reorientation time at room temperature was found to be 9-12 ps, based on nuclear magnetic resonance measurements [DDE96]. Detailed analysis of X-ray diffraction measurements on single crystals of $C_{60}$ were showing some orientational correlations between adjacent $C_{60}$ molecules at room temperature, consistent with a model of rapid ratcheting motion [MLR97, RLM96, SCK92]. The monolayer of $C_{60}$, is rotationally frozen on different substrates, like Cu(111), Al(111), Cu(110), Al(001), Cu(110), Ag(001) [FAA96, FAA99, CFS01] and possibly even on graphite [Li99], which was shown by X-ray photoelectron diffraction. The molecules have well defined orientations on the substrates, e.g. with a hexagon facing the surface on Cu(111) and Al(111), with the 5-6 bond on the Cu(110) surface or a single edge atom facing the Al(001) substrate. Taking into consideration the ratcheting of the rotation, we can conclude that the rotation of the $C_{60}$ molecules in the overlayers will only gradually increase in frequency, so that for the first few layers close to the rotationally frozen first monolayer the rotation will be much slower than the reported value measured for $C_{60}$ crystals.

We thus have two effects playing together for the suppression of the polymerisation in the proximity of substrates: one is the faster decay of the self-trapped state of the CT exciton, the other is the hindering of the rotation of the molecules, due to the correlated rotation and the freezing of the ML onto the substrate. The favourable orientation for the reaction, with two double bonds parallel to each other, can thus not be realised within the lifetime of the self-trapped state of the CT exciton. The exact thickness threshold for the onset of photopolymerisation can not be deduced from optical measurements, where the overall signal can be dominated by the not-transformed layers. Scanning probe techniques should be more appropriate for such a study.

# 2.6 The phototransformation of air-exposed $C_{60}$ films

## 2.6.1 Kinetics of phototransformation

Films of $C_{60}$ exposed to oxygen are known to show a hardening against photopolymerisation [ERZ95]. We studied the phototransformation of films with a thickness of 650 ML kept in air (and in darkness) for a few days by SHG. We observed that the Nd:YAG laser also has an influence on the processes induced by the $Ar^+$ irradiation in these films. Fig.2.22a shows the evolution of the SH signals with the $Ar^+$ irradiation, while the curves in Fig.2.22b correspond to steps of irradiation with $Ar^+$ laser followed by one minute Nd:YAG laser irradiation. The dose constants obtained from biexponential fits are 0.01 and $1.8 \cdot 10^{20}$ photons/cm$^2$ for Fig.2.22a, 0.01 and $2.3 \cdot 10^{20}$ photons/cm$^2$ for Fig.2.22b and the saturation levels are most strikingly different for the s-p signals (125% for Fig.2.22a and 95% for Fig.2.22b). The evolution of the SH signal is very different compared to the 650 ML films irradiated in situ, where the dose constants were 0.5 and 8.7 x $10^{20}$ photons/cm$^2$, and the saturation level of the s-p signal was 20% (see Section 2.5.2).

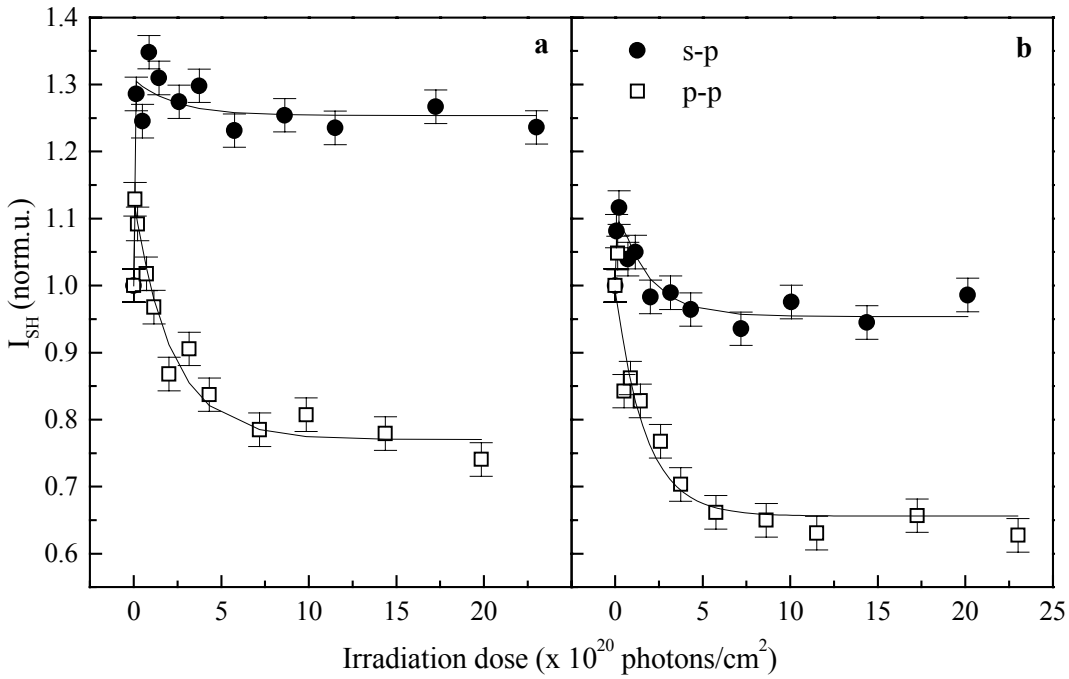


*Fig.2.22. Evolution of the SH signals for (a) $Ar^+$ laser irradiation and (b) $Ar^+$ laser followed by one minute Nd:YAG laser irradiation of air-exposed $C_{60}$ films of 650 ML.*

Since the oxygen present in the film is known to hinder the photopolymerisation, the change in the SH signal, with significantly smaller irradiation dose constants compared to oxygen-free

films, must be induced by a different process in this case. A modification of the SH signal from an $Ar^+$ laser irradiated film due to Nd:YAG laser irradiation was also not observed for oxygen-free films. This modification was not observed without the $Ar^+$ laser irradiation. No evidence for reactions induced by the Nd:YAG laser was found from IR spectroscopy (see discussion below). The effect observed on the SH signal can be induced by the diffusion of impurities inside the film, which can affect the local optical constants.

## 2.6.2 IR spectroscopy

The FTIR spectra of two films prepared on KBr and irradiated in air are presented in Fig.2.23. The broad absorption between 690 and 1000 $cm^{-1}$, together with the more clear peak at 955 $cm^{-1}$ are arising from epoxidic species and indicate an onset of the fullerene oxidation [WWH96, CBS94]. A small shift of the $C_{60}$ $F_{1u}$ modes of 1 to 2 $cm^{-1}$ observed in these spectra is also in good agreement with the semiempirical calculations from Cardini et al [CBS94] for epoxidic $C_{60}O$. The weaker peak at 1050 $cm^{-1}$ is due to the absorption of C-O groups. The more narrow peaks at 707 and 798 $cm^{-1}$ correspond to polymeric modes, showing that both polymerisation and oxidation take place under $Ar^+$ laser irradiation.

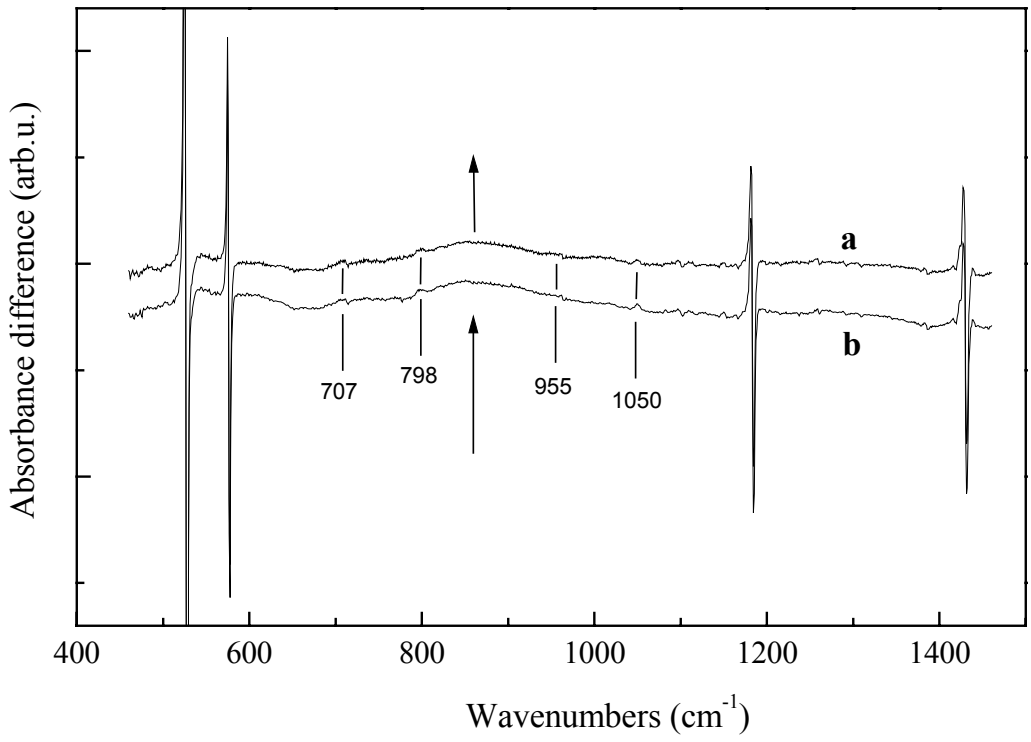


*Fig.2.23. Difference IR absorbance spectra of $C_{60}$ films irradiated in air after: (a) 10 minutes $Ar^+$ laser irradiation ($4.4 \cdot 10^{20}$ photons/$cm^2$) and (b) 10 minutes $Ar^+$ laser followed by one minute Nd:YAG laser irradiation.*

No significant difference after the Nd:YAG laser irradiation could be observed in the FTIR spectra, indicating that no reaction changing the vibrational properties of the molecules occurs under the effect of this laser.

## 2.7 Conclusions

Second harmonic generation using the fundamental wavelength of an Nd:YAG laser (1064 nm) is very sensitive to the initial phase of photopolymerisation of $C_{60}$. The transformation can be measured without interfering with the reactions. The phototransformation does not affect the crystallinity of $C_{60}$ films epitaxially grown on Ni(111) substrates, as shown from SH azimuthal anisotropy studies. Photopolymerisation with less than $10^{20}$ photons/cm$^2$ from an $Ar^+$ laser at 514.5 nm, first indicated by SHG measurements, was also confirmed with IR spectroscopy. This dose is much lower than previously reported from Raman spectroscopy. Considering an average day-light intensity of 400 W/m$^2$ in comparison with the irradiation times with 320 mW/cm$^2$ for the $Ar^+$ laser intensity used in our experiments, we can expect initial phototransformation already after 8 minutes of exposure to day-light in the $C_{60}$ films. The relatively strong transformation that we measured at these low doses may in part be attributed to the fact that oxygen impurities and overheating of the films during $Ar^+$ laser irradiation were carefully avoided. The presence of polymer modes at very low irradiation doses is suggesting a growth scenario around nucleation centers which refer to the structures described by the X-ray diffraction work of Pusztai et al. [POF99]. The thickness threshold behaviour for the onset of the polymerisation found in this work is in good agreement with the Raman spectroscopy measurements of Park et al. [PHK98]. It is consistent with a reaction mechanism having the self-trapped state of the charge transfer excitons as promoter of the polymerisation.

$Ar^+$ laser (514.5 nm) irradiation of air-exposed films of $C_{60}$ leads mainly to the oxidation of the molecules. The photopolymerisation is hindered by the presence of oxygen impurity and only weak peaks of the polymeric phase could be detected by IR spectroscopy on films irradiated with similar photon doses as the ones used for the oxygen-free films. For the oxygen-containing films, the Nd:YAG laser has an influence on the reaction kinetics, which we interpret as an enhanced diffusion of the oxygen in the depth of the film.